Electrical Power and Energy Systems 136 (2022) 107737

Contents lists available at ScienceDirect

International Journal of Electrical Power and Energy Systems

journal homepage: www.elsevier.com/locate/ijepes

Thermal analysis of 8.5 MVA disk-type power transformer cooled by biodegradable ester oil working in ONAN mode by using advanced EMAG–CFD–CFD coupling

Michal Stebel [a,*], Krzysztof Kubiczek [b], Gustavo Rios Rodriguez [c], Michal Palacz [a], Luciano Garelli [c], Bartlomiej Melka [a], Michal Haida [a], Jakub Bodys [a], Andrzej J. Nowak [a], Pawel Lasek [d], Mariusz Stepien [d], Francisco Pessolani [e], Mauro Amadei [e], Daniel Granata [e], Mario Storti [c], Jacek Smolka [a]

[a] Department of Thermal Technology, Silesian University of Technology, Konarskiego 22, 44-100 Gliwice, Poland
[b] Department of Measurement Science, Electronics and Control, Silesian University of Technology, Akademicka 10, 44-100 Gliwice, Poland
[c] Centro de Investigación de Métodos Computacionales, CIMEC (UNL - CONICET), 3000 Santa Fe, Argentina
[d] Department of Power Electronics, Electrical Drives and Robotics, Silesian University of Technology, Krzywoustego 2, 44-100 Gliwice, Poland
[e] Tadeo Czerweny S.A., 2252 Gálvez, Argentina

ARTICLE INFO

Keywords:
Power transformer
Biodegradable oil
Cooling system
Computational fluid dynamics
Electromagnetic
Coupled problem

ABSTRACT

Power transformers are the first devices used to transfer the electrical energy produced in power plants to the grid to supply the industrial and individual receivers with electricity. The heat generation in windings and core, being an effect of the power losses, is usually dissipated in large units by using mineral oils, which are harmful to the environment. Nowadays, the industry and global society seek environmentally-friendly alternatives. One of the most promising substitute for their high biodegradability, safety in operation, and favourable thermo-physical properties are natural ester oils. For this reason, a numerical study of 8.5 MVA disk-type power transformer cooled using conventional mineral oil and a commercially used rapeseed ester oil is presented in this paper. Moreover, due to different thermal behaviour of the considered oils, the comparison was made for the unit working in different seasons of hot and moderate climate zones (Argentina and Poland). In the numerical approach, electromagnetic (EMAG) and computational fluid dynamics (CFD) models were used for a detailed study of the selected device. In particular, a novel and very efficient EMAG–CFD–CFD coupling procedure was developed to assess the cooling of the large power transformer. Such a coupled computational procedure allowed for the detailed investigation of the power loss, oil flow characteristics, and temperatures with a satisfying computational effort. The results showed that the average windings temperatures are higher by 2–9 K when the ester oil is used, dependent on the ambient conditions. The hotspot temperature in the low voltage windings increased by up to 9 K and up to 18 K in the high voltage windings using ester oil. According to the results, the oil duct construction requires modification in the high voltage region for transformers cooled using mineral oil in cold climate conditions.

1. Introduction

Power and distribution transformers are crucial for the electricity distribution from the power plant to the end-users, both industrial or domestic. Although they have very high energy efficiency (>99%), part of the electrical energy is wasted as heat mainly due to the ohmic losses within the conductors and eddy currents within the magnetic core. In large units, cooling of these components is commonly realised using dielectric oil. Effective heat dissipation to the ambient is crucial because transformer reliability and life expectancy generally are dictated by hot-spot temperature (HST). Excessively high temperature accelerates the ageing rate of the insulation, which, as a consequence, may lead to the operation failure of transformers or any other electrical devices and machines [1]. According to the IEC 60076-7 standard [2], a temperature increase by 6 K may lead to a doubling of the insulation materials ageing rate. The issue of transformer insulation lifetime prediction was studied by Abu-Elanien and Salama [3]. The authors proposed a method based on Monte Carlo approach to predict the

* Corresponding author.
E-mail address: michal.stebel@polsl.pl (M. Stebel).

https://doi.org/10.1016/j.ijepes.2021.107737
Received 14 April 2021; Received in revised form 30 September 2021; Accepted 19 October 2021
Available online 5 November 2021

Nomenclature

$\bar{\boldsymbol{A}}$	Complex magnetic vector potential, T m
$\bar{\boldsymbol{B}}$	Complex vector of magnetic flux density, T
B	Length of vector of the magnetic flux density, T
c_p	Specific heat, J kg^{-1} K^{-1}
D	Cross-diffusion term, kg m^{-1} s^{-3}
f	Frequency, Hz
G	Generation term, kg m^{-1} s^{-3}
$\boldsymbol{g}$	Gravitational acceleration vector, 9.81 m s^{-2}
H	Length of vector of the magnetic flux intensity, T
h	Heat transfer coefficient, W m^{-2} K^{-1}
I	Current, A
$\bar{\boldsymbol{J}}$	Complex current density, A m^{-2}
j	Imaginary number, –
K	Kinetic turbulent energy, m^2 s^{-2}
k	Thermal conductivity, W m^{-1} K^{-1}
k_c	Coefficient of Eddy-current loss in Steinmetz's equation, –
k_e	Coefficient of Bertotti's excess loss in Steinmetz's equation, –
k_h	Coefficient of hysteresis loss in Steinmetz's equation, –
L	Reference length, m
l	Length, m
P	Power losses, W
p	Pressure, Pa
q	Heat flux, W m^{-2}
q_v	Volumetric heat source, W m^{-3}
$\mathbb{R}$	Real number
S	Cross section area, m^2
T	Temperature, K
Y	Dissipation term, kg m^{-1} s^{-3}
Z	Impedance, Ω
$\boldsymbol{w}$	Velocity, m s^{-1}
Gr	Dimensionless Grashof number
Nu	Dimensionless Nusselt number
Pr	Dimensionless Prandtl number
Ra	Dimensionless Rayleigh number

Greek Symbols

β	Coefficient of thermal expansion, K^{-1}
Δ	Difference
ε	Emissivity, –
μ	Dynamic viscosity, Pa s
μ_M	Magnetic permeability, H m^{-1}
ν	Kinematic viscosity, m^2 s^{-1}
ϱ	Density, kg m^{-3}
σ_r	Stefan–Boltzmann constant, 5.67e−8 W m^{-2} K^{-4}
σ	Electrical conductivity, S m^{-1}
ω	Specific dissipation rate, s^{-1}
ω_f	Angular frequency, rad s^{-1}

Abbreviations

CFD	Computational fluid dynamics
$EMAG$	Electromagnetic
FEM	Finite element method
FVM	Finite volume method
HST	Hot-spot temperature
HV	High voltage
LES	Large eddy simulation
LV	Low voltage
$ONAF$	Oil-natural air-forced
$ONAN$	Oil-natural air-natural
RMS	Root mean square
$THNM$	Thermal-hydraulic network model

Subscripts

amb	Ambient
$conv$	Convection
rad	Radiation
sur	Surface

expected lifetime of transformers based on their loading and ambient conditions.

For decades, mineral oils produced mainly from petroleum products were used as coolants and insulators in such applications. Their sustainable production and use are questioned nowadays due to limited natural resources and low biodegradability (less than 30%). This kind of oil has numerous drawbacks like a low flash point, low fire point, or possible significant contamination of soil and water in case of the oil leakage [4]. Undoubtedly, mineral oils are considered environmentally harmful. For this reason, biodegradable synthetic and natural ester oils are recognised as a promising alternative to mineral oils [4,5]. Commercially used natural oils for transformer cooling are products based on rapeseed, soybean, sunflower, palm, etc. [6]. They are identified with a high biodegradability level (over 95%), high flash point (>300°C), high fire point (>300°C) and low toxicity [4,6]. Due to these advantages regarding the safe operation and environmentally-friendly life cycle, which is crucial nowadays, these types of oils have a considerable potential to replace mineral oils globally. What is more, Cilliyuz et al. [7] pointed out that from the economical point of view, using natural oils can be beneficial especially for high-power transformers.

However, due to the high viscosity of natural oils, their cooling capabilities are lower, which may be a fundamental limitation for their utilisation as coolants for electrical devices. Moreover, the ageing of natural oils even further reduces their cooling capacity [8]. Another drawback of ester oils is their higher affinity for moisture in comparison to mineral oils, which affects the ageing rate and the transformer life cycle [9]. Despite these issues, there is still high interest in research regarding natural ester coolants. Even a cooking waste oil was introduced as an attractive alternative coolant due to its low price and the idea of sustainable use of natural resources [10].

To predict the HST, different methods based on physical phenomena modelling at different level of complexity were proposed by the researchers. For example, Zhou et al. [11] presented a simple and general model of the HST rise based on the heat transfer and hydrodynamic principles. Due to the use of basic algebraic equations based on the well-known fluid flow and heat transfer formulas, the proposed model represented the thermal behaviour of the transformer without high computational requirements. Radakovic et al. [12] developed a dynamic thermal model characterised by a similar level of complexity. They analysed the temperatures occurring inside a kiosk distribution transformer under changing weather conditions during the day. Taghikhani and Gholami [13] presented a different approach based on the finite element method (FEM) and a heat transfer theory.

Their model was based on a numerical solution of one partial differential equation for heat conduction. Rommel et al. [14] presented an alternative approach. They proposed a method to evaluate HST and assess the transformer lifespan based on the operator's electrical parameters. The authors of the studies mentioned above highlighted that their methods are convenient and relatively straightforward. Measured parameters can be useful also in another way to improve transformers operation reliability. Shiravand et al. [15] recently developed a thermal model based on several measured temperatures for the early detection of faults in the transformer operation. Such studies are undoubtedly beneficial, but for a detailed description of the internal temperature distribution of the transformer, more complex methods have to be used.

The most common practice used for detailed analyses of these devices is to discretise the transformer geometry to develop numerical models describing the electromagnetic, heat transfer, and fluid flow phenomena occurring in the transformer, usually as a coupled solution. The first step in such a strategy is to assess the losses in the magnetic core and windings. A popular method for that is the electromagnetic (EMAG) simulation based on FEM. Numerous studies to evaluate spatial-distribution of power losses for further thermal simulations have been performed, e.g., the coupled analysis by Smolka et al. [16], where the EMAG results were defined as local heat sources in the computational fluid dynamics (CFD) model. Numerous similar studies of the author's work followed this study. They pointed out that performing coupling electromagnetic and heat transfer analyses is reasonable and effective, e.g., because the EMAG simulations do not need as complex discretisation as CFD modelling. If the spatial-distribution of losses is not required, FEM simulations may be replaced by more straightforward methods, e.g., the analytical calculation presented by Eslamian et al. [17].

A popular approach for the fluid flow and heat transfer analyses of electrical devices is developing the thermal-hydraulic network model (THNM) for the unit. Rahimpour et al. [18] pointed out that this method is more advantageous than CFD modelling in terms of computational efficiency. Although the authors claim that their THNM model predicts disk temperature with an uncertainty of less than 3 K (which is fairly acceptable in engineering applications), they could compute only constant and one-dimensional velocity values of the oil within the cooling ducts which is a significant simplification of the oil flow physics. The same two methods are employed by Santisteban et al. [19] to assess the HST value in disk-type transformer windings cooled by both mineral and natural oils. Torriano and Chaaban [20] compared CFD and THNM methods and highlighted their pros and cons. According to the authors, CFD requires more computational effort. However, despite this inconvenience, a well-developed CFD model follows the fundamental flow phenomena even on a small scale. Therefore, it allows for characterisation of the temperature, pressure, and velocity fields in detail to better understand the fluid phenomena occurring within the complex structure of disk-type windings of the transformer. Similar conclusions were drawn by Skillen et al. [21], who highlighted that some local effects might occur inside the transformer windings, and only CFD can represent them accurately.

Because of the high computational requirements, the CFD technique is usually employed to analyse a selected component of the power transformer, e.g., windings, where the HST evaluation is crucial or radiators, which should ensure efficient heat dissipation. Also, numerous simplifications are commonly introduced to the models, i.e., reducing the domain dimensionality to 2-D, axisymmetric 2-D, or a repeatable 3-D segment of windings as well as the homogenisation of the insulated conductors. Moreover, the physics of the heat transfer or fluid flow is often simplified, e.g., the buoyancy force is neglected. Torriano and Chaaban [20] studied the parameters affecting the temperature distribution in the disk-type transformer and compared the commonly used simplifications. According to their results, a buoyancy force should be included even if the oil flow is forced but an appropriate simplification, namely the Boussinesq approximation for the density change effect on the body forces, is reasonably acceptable. The domain reduction is a common solution to reduce the geometrical complexity of the model. Gastelurrutia et al. [22] simplified a full 3-D domain of the distribution transformer into a thin slice that covers a part of the windings and one fin. For transformer windings modelling, formulating a 2-D axisymmetric domain is rather common. However, according to Torriano and Chaaban [23], three-dimensional flow phenomena occur within the transformer windings. Moreover, the duct spacers presence affects the heat dissipation from the conductors, therefore such analyses should be performed using a 3-D domain. Simplification of the domain into a 3-D repeatable segment seems to be a reasonable strategy as done by Eslamian et al. [24], who developed a CFD model covering one-eighth of the windings. In such a way, all the geometric details can be included in the domain, and a three-dimensional flow character can be modelled.

Other studies are dedicated to analysing the external radiators, which dissipate heat from the hot oil to the ambient air. Rios Rodriguez et al. [25] employed both the analytical and numerical methods to determine the heat transfer coefficients and transformers radiator cooling capacity working in an oil-natural air-natural (ONAN) cooling regime. Large eddy simulation (LES), a more advanced CFD methodology, was employed in this study to obtain more accurate results. The authors extended their model with oil-natural air-forced (ONAF) cooling mode and, as an effect, developed a tool that allows for the parametric study, useful for the radiator design process [26]. Their results were in good agreement with the experiments. A similar study focused on the numerical evaluation of radiator performance was done by Kim et al. [27], where the authors analysed different arrangements of fans attached to the radiators. Such studies are helpful and useful to define efficient arrangement of power transformer radiators and, as a result, improve their design.

Parametric and variant studies may be used to optimise the construction of selected elements of the transformer or the whole unit itself. Raeisian et al. [28] performed the CFD analysis of the 200 kVA distribution transformer cooled in ONAN regime and identified the geometrical parameters affecting HST mostly. In this study, response surface methodology was used to optimise the geometry of the device. Smolka and Nowak [29] employed a genetic algorithm and coupled EMAG–CFD simulations to optimise the diameter of cooling ducts and coils in a dry-type transformer using 2-D axisymmetric geometry. They proposed a modified construction of the windings that would allow for the HST reduction by 10 K. This work was extended into a more detailed 3-D geometry in the next step [30]. As seen, although these CFD simulations are considered computationally demanding, they can be used for parametric study and optimisation with good results if the numerical model is formulated with a reasonable level of detail.

The aim of this study is twofold. Firstly, to present a novel strategy for effective numerical simulations by coupling the EMAG and two CFD models of different components of a large power transformer or similar units and systems, where this methodology may be applied. In this way, a computational effort to obtain accurate results may be significantly reduced by performing the separate simulations of characteristic parts of one unit simultaneously. Secondly, to compare the temperature fields and HST inside the components of disk-type power transformer cooled by mineral oil and the natural ester oil, what was not performed using such a detailed numerical model yet. This analysis covers several scenarios of the transformer performance at different ambient conditions. These are the summer and winter temperatures characteristic for two climate zones, i.e., a warm climate in Argentina and a moderate climate in Poland, including the typical hottest and coldest temperatures. The results can be treated as the assessment of the possible advantages and disadvantages of using alternative and environmentally friendly natural oils instead of commonly used mineral oils.

In this paper, the coupled EMAG–CFD–CFD model is presented to accurately simulate the thermal behaviour of the 8.5 MVA disk-type power transformer. This unit is cooled using external radiators working

Table 1
Main parameters of the 8.5 MVA power transformer.

Rated power	8.5 MVA
Rated voltage HV	33 kV
Rated voltage LV	6.9 kV
HV regulation	± 2 × 2.5%
Type of cooling	ONAN
Connection symbol	Dyn11
HV winding wire	Rectangular
Quantity of disks HV	58
LV winding wire	Rectangular
Quantity of disks LV	50 (gap)
Magnetic core type	3 limbs

in the ONAN regime, whose performance was represented using the reduced model by Rios Rodriguez et al. [25], adjusted to this particular transformer manufactured by Tadeo Czerweny. The EMAG simulations were performed to evaluate the spatial distribution of heat losses within the transformer windings and the magnetic core. The losses are used as volumetric heat sources in two coupled CFD–CFD models. One represents a repeatable segment of windings, while the second accounts for the oil bulk flow inside the transformer interior. This method allows for the effective performance of the CFD simulations in a reasonable computational time that is much shorter when compared to the model that contains all the details of the considered unit. To the best authors' knowledge, such a methodology was not proposed before for the CFD simulations of the power transformers.

2. Description of the power transformer

The unit analysed in this study is an 8.5 MVA power transformer with a rated voltage of 33/6.9 kV/kV working in the ONAN cooling regime as presented in Fig. 1. The unit is manufactured by Tadeo Czerweny S.A. company from Galvez, Argentina. It is equipped with 8 external radiators, each consisting of 18 panels. Each panel is 1.4 m high and 0.5 m wide. Internal dimensions of the transformer interior are approximately 2.4 m (width), 2.1 m (height), and 0.94 m (depth). Table 1 shows the main parameters of this unit.

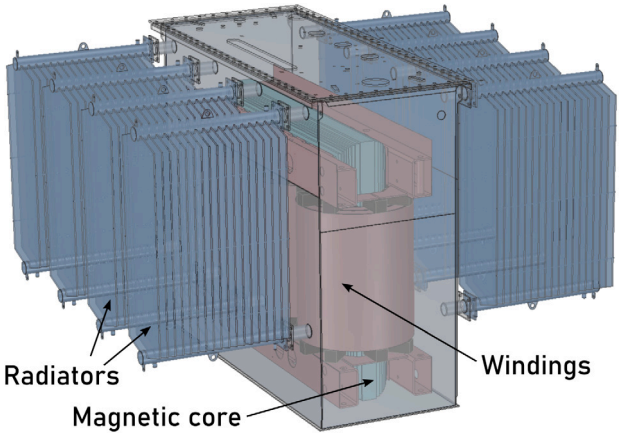

Fig. 1. General scheme of entire power transformer with naturally cooled external radiators.

The disk-type windings are organised as follows, 58 disks on the high voltage (HV) side and 50 disks on the low voltage (LV) side. It is worth mentioning that an additional gap separates the turns of wires in each LV disk. Therefore, there are two vertical oil ducts on the HV side and three ducts on the LV side within the windings. One more duct is present between the core limb and the inner part of windings. The transformer features a de-energised tap changer at the HV winding in the range of ±2 × 2.5% of the rated voltage. Therefore, two HV disks (29th and 30th) are not active at the nominal tap position.

In large power transformers, washers are usually used between every few disks to control the oil flow. Their presence forces a zig-zag flow of the oil, resulting in enhanced cooling of conductors [18]. In the transformer being the subject of this paper, no washers are used. Therefore, it is expected that the horizontal component of the oil velocity will not be significant in the gaps between disks, and the temperatures of disks may be relatively high as the vertical oil flow is only designed for this unit.

3. Formulation of the coupled EMAG-CFD-CFD numerical model

3.1. General assumptions of coupled modelling

As mentioned in the introduction, the methodology proposed for the numerical prediction of the transformer cooling is based on coupling a few sub-models. These are: (1) the EMAG model, which is used to correctly evaluate the distribution of power losses within the magnetic core and within the windings; (2) transformer windings CFD model, which accounts for a detailed analysis of the oil flow within the segment of one phase winding; (3) tank CFD model used for a correct prediction of cooled and heated oil circulation within the transformer tank simplified to 1/4th of the entire geometry of this transformer part. For the different numerical models, the geometries of transformer parts were prepared for each model in a different way. Fig. 2(a) presents the top view of the power transformer geometry before any simplification. For EMAG simulations, half of the core and half of each phase windings shown in Fig. 2(b) was necessary to be included in the analyses. In the windings CFD model, to achieve a satisfying level of 3-D heat conduction and fluid flow prediction, the repeatable segment of one phase windings were included in the analyses, as shown in Fig. 2(c). The tank CFD model was simplified to analyse a quarter of the transformer tank interior as presented in Fig. 2(d). The latter model does not analyse the windings, which are included in the separate CFD model. Also, the heat transfer and the fluid flow through the radiators are not analysed by using the CFD method in this study but are represented using a reduced model. Computational domains of each numerical model will be discussed in detail in Section 3.2.

The coupling of all the numerical models is an essential aspect of the analysis presented in this paper. Firstly, the coupling between the EMAG model and both CFD models is realised in a manner common for such studies, i.e., by implementing the power losses distribution computed with the EMAG model, as volumetric heat sources within the core and windings in CFD models. The coupling between both CFD models for fluid flow and heat transfer analysis is performed differently. It is based on pairing the correspondent boundary conditions defined in separate models but at the same physical surface in the transformer geometry. During the computational process, the data exchange is realised between these pairs of boundary conditions, and as an effect, the agreement is achieved between two converged models. The computational procedure is described in Section 3.4 while Section 3.8 describes the formulation of the boundary conditions in detail.

3.2. Computational domains

In the EMAG simulations, the analyses are focused on the active parts, i.e., the magnetic core and the windings. These components take part in the magnetic induction phenomena, and the electrical energy conversion and heat are mainly generated within these components.

In this study, three different geometrical domains characterised by a different level of complexity were considered for the power losses evaluation. These domains are (1) 2-D domain with fully homogenised windings (2) 2-D domain with the homogenisation of each separate disk, and (3) 3-D domain with fully homogenised windings which includes 1/2 of the core and the windings. Also, an attempt was made to develop a considerably more complex geometrical domain,

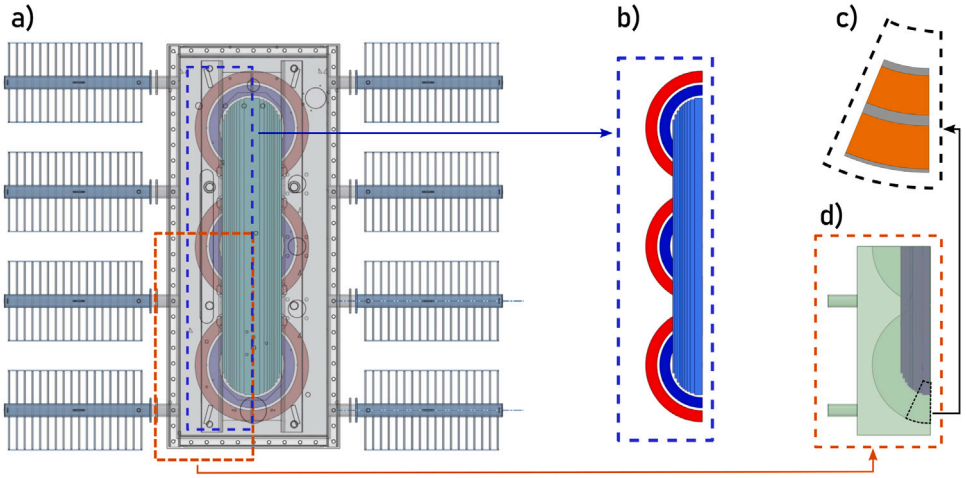

Fig. 2. Scheme presenting (a) the full geometry of the analysed unit, (b) part of the transformer analysed in EMAG model, (c) part of the transformer analysed in the tank CFD model and (d) part of the windings analysed in the windings CFD model.

i.e., the 3-D domain with the homogenisation of each disk. However, the computational effort was huge and not justified for the final EMAG analyses when this domain was used. In geometrical domains (1) and (3) with full homogenisation of windings, all the LV and HV disks were merged. It was possible by assessing the filling factors considering the actual volume of conductors. Eventually, the 3-D domain (3) with the full homogenisation of windings was selected for the EMAG simulations. Firstly, because according to the comparison of two 2-D domains results, a full homogenisation does not cause any significant error and secondly, because this 3-D model still guarantees a reasonable computational time.

The geometrical domain of the selected 3-D EMAG model is presented in Fig. 3. It should be pointed out that two of the HV disks are not active during the nominal operation of the transformer (disks number 29 and 30 counting from the bottom). Therefore, only a small amount of heat losses is generated within them, related with the eddy losses induced by the magnetic leakage flux.

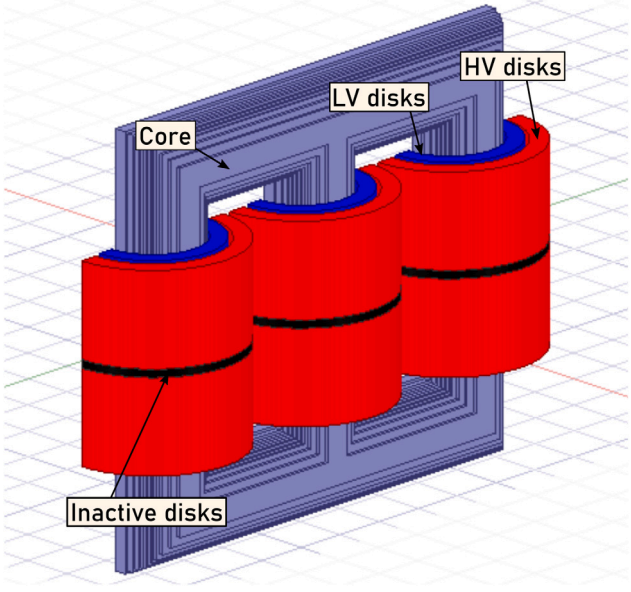

Fig. 3. Geometrical domain of 3-D EMAG model representing a half of the transformer active parts.

In the case of the CFD simulations, the computational domain is required to be much more detailed. Smolka and Nowak [31] reported that a difficulty in the CFD model development of such a device is a different level of length scales, resulting in a considerable size of the numerical mesh. The unit itself is relatively large, while small-scale flow patterns are significant in some of its parts at the same time. For that reason, two separate models were developed for the representation of the whole unit: (1) the CFD model of the windings used to simulate the complex oil flow in the disk-type windings structures, including the small gaps between disks and to estimate the local temperatures in every HV and LV disk, and (2) the CFD model of the transformer tank used to represent the flow of the oil inside the transformer tank for the accurate assessment of the oil temperature in every part of the unit and the distribution of the oil cooled by using the radiators within the transformer.

As mentioned, the CFD windings sub-model shown in Fig. 4(a) was developed to accurately simulate the complex flow of the oil inside the horizontal and vertical oil ducts, which are shown in Fig. 4(b). This model is crucial because the HST assessment within the windings requires a detailed representation of such complex geometry. The computational domain of the windings model includes a detailed 3-D geometry of a repeatable segment of one-phase windings. The similar approach was selected in a different CFD analysis reported in the literature [24] and is identified as the proper one regarding the computational time and the accuracy of the model. The selected segment deals with 1/16th slice of the whole windings around a single core limb. The slice is imposed by the presence of radial separators that significantly affect the oil flow pattern in this transformer part. In this CFD model, each disk is represented as a homogenised solid. As discussed before, the LV disks are separated; therefore, an additional oil flow through the vertical duct is present. Moreover, the core limb volume was reduced to a cylindrical surface with a properly defined boundary condition, discussed in Section 3.8. For example, this kind of simplification was already used by El Wakil et al. [32], where the authors represented the volume of the core and the windings by using an adequately defined boundary condition.

The computational domain of the second CFD model, i.e., the tank model, is presented in Fig. 4(c). It represents 1/4th of the transformer interior, which is a commonly used simplification in such studies, e.g., in [31]. It is possible due to the symmetrical geometry of the unit. It is essential to notice that the windings and the core limbs are removed from this domain, whereas the windings geometry model contains these components. Due to that, the domain of the tank model could be defined with a reasonable level of complexity. Most of the domain is occupied by oil. However, the top and the bottom yokes (and some minor parts of the core limbs) are present in the domain because they are not included in the windings model. It is worth mentioning that two large bars used to support the transformer core and windings

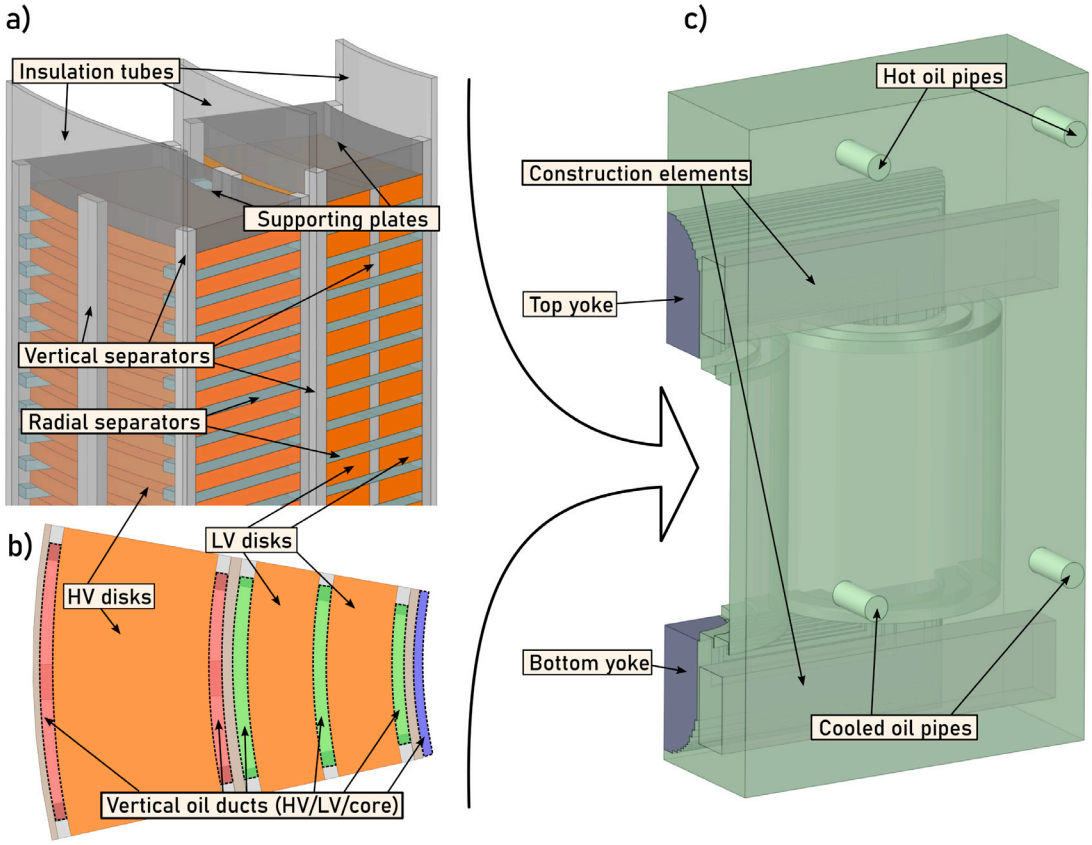

Fig. 4. Geometrical domain of: (a) windings CFD model in isometric view including: LV and HV disks, insulation tubes, vertical and radial separators and supporting plates, (b) the oil gaps between the solid parts in the cross-section and (c) tank CFD model which includes: the oil domain of the transformer interior and the oil pipes, major construction elements, top and bottom yokes.

were included in the geometrical domain because they affect the oil flow just above and below the windings.

As seen in Fig. 4(c), radiators are not included in the computational domain of the transformer CFD model presented in this study. Their performance and cooling capacity were evaluated using the semi-analytical model described in previous studies [25,26] and adjusted to the particular geometry of the unit and different ambient conditions analysed in this work. This aspect will be discussed in detail in Section 3.8.5. The oil flows geometric domain includes only a part of the pipes through which the hot oil flows from the transformer to radiators and back to the transformer interior after cooling down.

3.3. Numerical mesh

For the EMAG analysis based on FEM, the discretisation is not as rigorous as for fluid flow modelling. Firstly, the physical phenomena are not as small-scale as the fluid flow, and secondly, because the geometry of copper and magnetic steel elements is relatively simple. Moreover, the EMAG model used in this study is represented by the simplified winding approach due to their homogenisation. The cooling oil has negligibly small magnetic permeability compared to that of the magnetic steel used for the transformer core. Due to this fact, the magnetic flux is enclosed within the core, so the coolant mesh does not need to be fine to keep a high degree of accuracy. The adaptive meshing tool was chosen. At the beginning of the meshing procedure, the maximum element size had been set as equal to 15 and 40 mm for windings and core, respectively, which resulted in around 200 k elements. Then, the meshing tool made mesh refining iterations. Each iteration increases the number of mesh elements by about 30% until the relative change of energy between refinements is less than previously set 0.1%. As a result, the domain of the disks and the core for the EMAG simulation was composed of about 1.2 M elements.

The discretisation of the transformer geometry was performed separately for both CFD models using different strategies. For the windings CFD model, the numerical mesh was performed using ICEM CFD software and a blocking technique, allowing the authors to prepare a high-quality structured mesh composed of hexahedral elements only. Fig. 5(a) presents a numerical mesh in a vertical cross-section of a full 3-D windings geometry. Because the dimensions and number of the LV and HV disks are different, an interface was used in the middle of the insulation tube between both sides. Additionally, the mesh has been refined within the fluid region to improve the discretisation accuracy. As a result, the total number of cells is approximately 2.8 M for the CFD windings model.

The geometric discretisation of the tank model was realised in a different manner. The ANSYS Meshing software was used to prepare a hybrid mesh composed of tetrahedral and hexahedral elements in different regions presented in Fig. 5(b). Tetrahedral elements allowed for the generation of the high-quality mesh between the elements of various shapes, e.g., within narrow gaps between coils or between the yokes and construction bars included in the domain of this model. Additionally, it was beneficial for transition regions between coarse and fine hexahedral zones. Hexahedral elements were preferable for the yokes volume discretisation and some of the fluid regions, i.e., near external walls, along the outer surface of windings, and near the inlet and outlet boundary conditions, as presented in Fig. 5(c). The pipes for the oil flow from and to the radiators were meshed with hexahedrals as well. The mesh of this CFD model was composed of nearly 11 M cells in total.

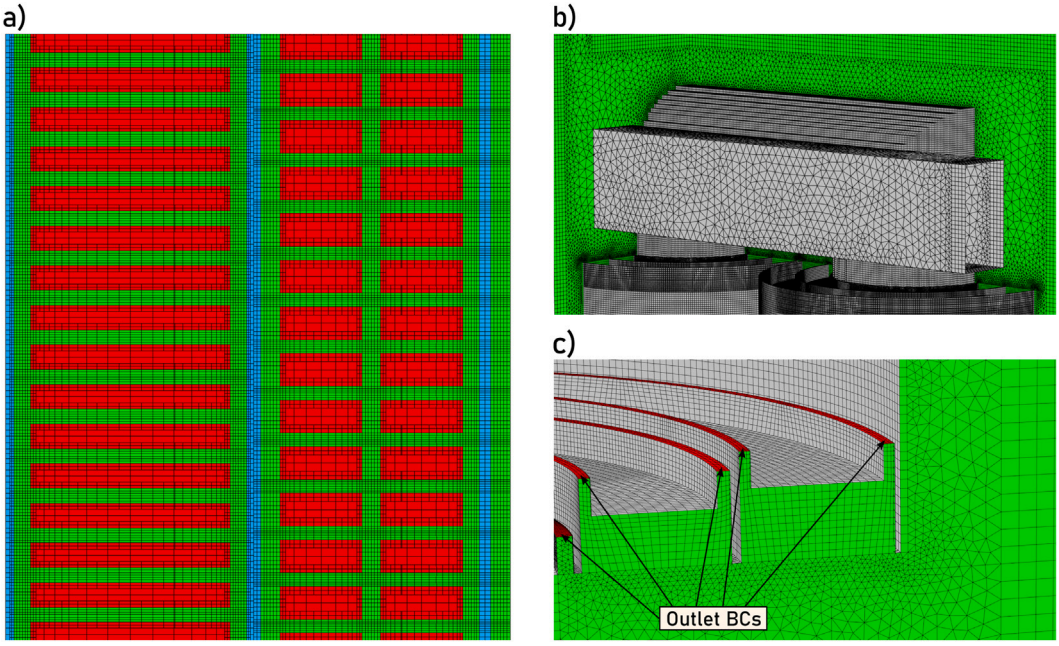

Fig. 5. Numerical mesh of (a) windings model presented in a vertical cross-section, (b) area of the top yoke in the tank model and (c) area of external surfaces of bottom part of windings in tank model.

3.4. Computational procedure

The flow chart of the whole coupled computational process is presented schematically in Fig. 6. The first step of the computational procedure was the EMAG simulations which resulted in a volumetric distribution of the power losses in the magnetic core and all active disks. For the sake of computational efficiency, the EMAG simulations were performed only once for the reference core and windings temperatures (core: 70°C; LV: 71.7°C; HV: 78.5°C). The resulting volumetric heat sources are temperature-dependent; therefore, they were corrected in the CFD model based on the local temperatures, taking into consideration the known temperature dependency of losses in copper and in the iron.

The first step of coupled CFD–CFD simulations was to start the windings model based on the assumed temperature values set as boundary conditions. After the initial solution was obtained, the tank CFD model computation process was started. At that time, both models were being solved separately and simultaneously. The temperature, the oil mass flow rate, and other quantities at the corresponding boundary conditions were transferred between both models after 100–200 iterations during the computational process until the agreement between both models was achieved. A simple in-house code managed the data transfer between both CFD models. During the simulations, CFD software was reading the input data from and exporting the output data into the external files every 100 iterations for the windings model and every 200 iterations for the tank model. The developed in-house code performed the input/output data transfer operation between these files every minute. Section 3.8.5 covers a detailed description of the physical quantities exchanged and defined at the corresponding boundary conditions of both models. The computational process was considered as completed when both CFD models were converged, and the physical quantities exchanged between them were stabilised, i.e., when all the transferred values of the temperature were changing by less than 0.2 K during the last 5 data exchange operations. The coupled CFD–CFD simulations were performed using a computer equipped with Intel Core i7-9700 CPU 3.00 GHz (30 cores) and 128 GB RAM. Each coupled simulation took approximately 4 days to be converged, which was strongly sensitive to the physical conditions assumed during the initialisation step. Taking into consideration the physical complexity of the problem, i.e., the properties and heat sources temperature-dependency, the multi-scale flow of the oil, and the natural convection phenomena, this computational time is fairly satisfying.

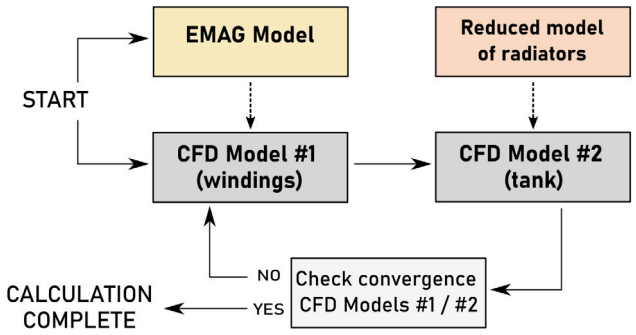

Fig. 6. Flow chart of the computational procedure for the coupled EMAG–CFD–CFD simulation.

3.5. Governing equations

To compute the time-varying magnetic field, the EMAG model was performed by ANSYS *Maxwell* module using *Eddy-current* solver, which allows for the time-harmonic eddy-current analysis. The total losses of the transformer can be separated into windings (Ohmic) loss and core loss. As the first step of EMAG loss analysis, winding losses are performed. The amplitudes of the current flowing in the primary and secondary windings, at the rated transformer parameters, are given by the transformer manufacturer. Thus, it is convenient to apply the harmonic current sources with well-known amplitudes in both the primary and secondary windings. The power losses generated in the copper windings are computed from the Joule–Lenz law defined as:

$$P = I_{RMS}^2 \cdot \mathbb{R}(\bar{Z}) \tag{1}$$

where I_{RMS} is the root mean square or the current flowing in a particular winding, $\mathbb{R}(\bar{Z})$ is the real part of winding impedance, which

is expressed by:

$$\mathbb{R}(\bar{Z}) = \frac{l}{\sigma S} \tag{2}$$

where l is the length of a wire used to wound a winding, σ is electric conductivity, and S is the cross-sectional area of a wire.

The second step of transformer loss computation is its core loss. The core loss is dependent on magnetic field, computed from the Maxwell's equations, where the windings are previously assumed as a source of the time-harmonic magnetic field. Due to low frequency of the current, flowing in the transformer coils, the displacement current in the Ampere's law can be neglected. Therefore, to compute distribution of magnetic field in the core, it is necessary to solve set of equations [33]:

$$\nabla \times \frac{1}{\mu_M} \nabla \times \bar{\boldsymbol{A}} = \bar{\boldsymbol{J}} - j\,\omega_f\,\sigma\,\bar{\boldsymbol{A}} \tag{3}$$

$$\bar{\boldsymbol{B}} = \nabla \times \bar{\boldsymbol{A}} \tag{4}$$

$$\mu_M = \mu_M(\bar{\boldsymbol{B}}) \tag{5}$$

where $\bar{\boldsymbol{A}}$ is the complex magnetic vector potential, $\bar{\boldsymbol{J}}$ is the complex vector of the current density, j stands for imaginary number, ω_f is the angular frequency, μ_M is the magnetic permeability, $\bar{\boldsymbol{B}}$ is the complex vector of the magnetic flux density. The relationship between $\bar{\boldsymbol{B}}$ and μ_M is given by the manufacturer for the non-linear magnetisation characteristic.

Finally, the total core loss is defined by Steinmetz's equation [34]:

$$P = k_h\,f\,B^2 + k_c\,(f\,B)^2 + k_e\,(f\,B)^{1.5} \tag{6}$$

where k_h is the coefficient in the hysteresis loss term, k_c is the coefficient in the eddy-current loss term, k_e is the coefficient in Bertotti's excess loss term, f is the frequency, and B stands for the length of $\bar{\boldsymbol{B}}$ vector. The values of coefficients k are obtained from interpolation of loss vs. magnetic flux density ($P = \zeta(B)$) characteristic, given by manufacturers.

The oil flow and the heat transfer are solved in both CFD models in steady-state. They are defined by a set of equations describing incompressible flow in terms of mass, momentum, and energy conservation given in Eqs. (7)–(9).

$$\nabla \cdot \boldsymbol{w} = 0 \tag{7}$$

$$\varrho\,(\boldsymbol{w} \cdot \nabla)\,\boldsymbol{w} = \mu\,\nabla^2 \boldsymbol{w} - \nabla p + \varrho\,\boldsymbol{g} \tag{8}$$

$$\nabla\,(k \nabla T) + q_v = \varrho\,c_p\,(\boldsymbol{w} \cdot \nabla T) \tag{9}$$

where $\boldsymbol{w}$ is the velocity vector, ϱ is the density, μ is the dynamic viscosity, p is the pressure, $\boldsymbol{g}$ is the gravitational acceleration vector, k is the thermal conductivity, T is the temperature, q_v is the volumetric heat source and c_p is the specific heat capacity.

In the energy balance given in Eq. (9), a heat source term describes the overall losses generated within the windings and the core computed by Eqs. (1) and (6), respectively. The velocities of the oil flowing in the transformer are low, which in general leads to low Reynolds numbers being characteristic of the laminar flow. However, in the case of the oil flow within the regions of windings, local turbulence effects were assumed possible as mentioned in [21]. In the cited reference, the authors used a turbulence model for initial simulations but assumed laminar flow for subsequent simulations of the oil flow in windings equipped with washers. In the transformer analysed in this study, turbulence is able to develop along the whole vertical oil ducts within the windings. Consequently, Rayleigh number was determined considering the vertical oil duct height as a characteristic length. Its value was over 10^{11}, which justifies the assumption of the turbulent flow in that part of the transformer. For that reason, k-ω SST turbulence model was used in this CFD model because it is well known as appropriate for the duct flows and complex geometries [35]. Therefore, two additional equations are solved for the windings model, i.e., for the turbulence kinetic energy and the specific dissipation rate given in Eqs. (10) and (11).

For the second CFD model, the tank model, the flow was assumed as laminar. In this case, Rayleigh number of approximately 10^9 was reached locally near the top yoke. Such value suggests that the transition between the laminar and the turbulent flow regime can occur in that region. However, in all the other regions the flow is less intensive. For that reason, no turbulence approach was employed in that CFD model.

$$\varrho\,K\,(\nabla \cdot \boldsymbol{w}) = \nabla \cdot \left[\left(\mu + \frac{\mu_T}{Pr_K}\right) \nabla K\right] + G_K - Y_K \tag{10}$$

$$\varrho\,\omega\,(\nabla \cdot \boldsymbol{w}) = \nabla \cdot \left[\left(\mu + \frac{\mu_T}{Pr_\omega}\right) \nabla \omega\right] + G_\omega - Y_\omega + D_\omega \tag{11}$$

where K is the turbulent kinetic energy, μ_T is the turbulent dynamic viscosity, Pr_K is the turbulent Prandtl number for turbulent kinetic energy, G_K generation of turbulent kinetic energy due to mean velocity gradients, Y_K dissipation of turbulent kinetic energy due to turbulence, ω is the specific dissipation rate, Pr_ω is the turbulent Prandtl number for specific dissipation rate, G_ω is the generation of specific dissipation rate, Y_ω is the dissipation of specific dissipation rate due to turbulence, D_ω is the cross-diffusion term.

In both CFD models, a pressure-based solver was used in ANSYS Fluent software to obtain a steady-state solution of governing equations. Pseudo-transient approach was employed to get the converged solution more effectively. Second-order schemes were selected for spatial discretisation of the equations.

3.6. Material properties

For the development of numerical models, different material properties had to be defined for the solid materials and the oil. The properties of solid elements are listed in Table 2. For the EMAG simulations, the required properties to define the windings are the copper conductivity and copper mass density, which are well known in the literature. The former is strictly dependent on the temperature, with temperature coefficient typically assumed as equal to +0.37% per 1 K of the temperature rise. Similar dependence was reported in different studies dealing with electrical devices cooling and temperature-dependent loss estimation, e.g., [36]. In terms of magnetic core, electrical conductivity, mass density and stacking factor are given by the manufacturer. The manufacturer also provided $(B - H)$ magnetisation characterisation as well as $(P - B)$ power loss curve. Due to lack of information about P temperature coefficient, the typical linear dependence equal to −0.15% per 1 K of the temperature rise was assumed, which is correct in small changes of the temperature [37].

For the steady-state CFD simulations, the thermal conductivity of solid materials is needed. The windings and the core of the transformer are composed of layered materials (copper conductors and insulation for windings, steel, and varnish for the core). For that reason, the thermal conductivity of these elements is defined as an anisotropic quantity related to the heat conduction direction. The magnetic core is built of thin sheets of steel, each covered by the varnish, while the windings are composed of a number of rectangular conductors, separated by paper insulation. An analytical model can be utilised to evaluate thermal conductivity of layered materials as done in several similar studies, e.g., [16,31]. The effective thermal conductivity was evaluated in axial, radial, and tangential directions for the LV and HV disks separately and for the normal and tangential direction for the core. That analytical approach is based on the electrical resistivity analogy. It is described by Eqs. (12)–(13) for the parallel and perpendicular orientation of the layers, respectively.

$$k_i = l_i \sum_{j=1}^{n} \frac{k_j}{l_j} \tag{12}$$

$$k_i = \frac{l_i}{\sum_{j=1}^{n} \frac{k_j}{l_j}} \tag{13}$$

where k_i is the effective thermal conductivity in the ith direction, l_i is the dimension of the solid material in ith direction, k_j is the thermal conductivity of jth material and l_j is the dimension of the solid material layer in ith direction.

In addition, thermo-physical properties of the cooling oils are needed to simulate the heat dissipation employing CFD simulations. The required properties are density, specific heat, dynamic viscosity, and thermal conductivity. To assess the potential of the natural oils, two oils are used in this study. One of them is the mineral oil described by Santisteban et al. [38]. The second one is Midel eN 1204 rapeseed oil, used commercially. The latter one was compared by Salama et al. [6] with mineral oil and several different environmentally friendly oils in terms of their thermo-physical properties.

Thermo-physical properties were implemented in the CFD models as temperature-dependent parameters. Table 3 presents the formulas describing the mineral oil taken from the literature [38] while the Midel eN 1204 ester oil properties presented in Table 4 were determined by the authors based on the data from the oil producer.

The main difference between both oils regarding the flow and the cooling capabilities is the dynamic viscosity. For the ester oil, the dynamic viscosity is higher than that for the mineral oil, especially at low temperatures. Thus, the cooling may be less effective in winter conditions in cold climates if the ester oil is used. On the other hand, the thermal conductivity of the ester oil is significantly higher, which is beneficial for the heat dissipation from the heated elements of the transformer. All the used properties are presented for both oils in Fig. 7.

Table 3
Functions of temperature in K describing physical properties of the mineral oil [38].

Property	Function of the temperature
Density, kg m^{-3}	$1098.72 - 0.712 \cdot T$
Specific heat, J kg^{-1} K^{-1}	$807.163 + 3.58 \cdot T$
Dynamic viscosity, kg m^{-1} s^{-1}	$0.08467 - 4e{-}4 \cdot T + 5e{-}7 \cdot T^2$
Thermal conductivity, W m^{-1} K^{-1}	$0.1509 - 7.101e{-}5 \cdot T$

Table 4
Functions of temperature in K describing physical properties of Midel eN 1204 ester oil.

Property	Function of the temperature
Density, kg m^{-3}	$1109.8 - 0.6539 \cdot T$
Specific heat, J kg^{-1} K^{-1}	$1266 + 1.9757 \cdot T$
Dynamic viscosity, kg m^{-1} s^{-1}	$68\,397.18/(T^3 - 478.65 \cdot T^2 + 57\,268.59 \cdot T + 493.959)$
Thermal conductivity, W m^{-1} K^{-1}	$0.135 + 3.909e{-}4 \cdot T - 8.4688e{-}7 \cdot T^2$

Table 2
Physical properties of the solid materials used for EMAG and CFD simulations.

Transformer element	Physical property	Value
Windings	Electrical conductivity	58 MS m^{-1} @25°C
	Mass density	8933 kg m^{-3}
	LV thermal conductivity (rad/tan/ax)	2.52/307.0/10.5 W m^{-1} K^{-1}
	HV thermal conductivity (rad/tan/ax)	2.33/297.0/7.89 W m^{-1} K^{-1}
Magnetic core	Electrical conductivity	2.083 MS m^{-1}
	Mass density	7650 kg m^{-3}
	Stacking factor	0.95
	Magnetic permeability	$B - H$ curve
	Steinmetz core loss coefficients	$P - B$ curve @25°C
	Thermal conductivity (normal/tan)	14.5/48.9 W m^{-1} K^{-1}
Separators, insulation tube	Thermal conductivity	0.2 W m^{-1} K^{-1}
Tank, construction	Thermal conductivity	28.0 W m^{-1} K^{-1}
Tank outer surfaces	Emissivity	0.98

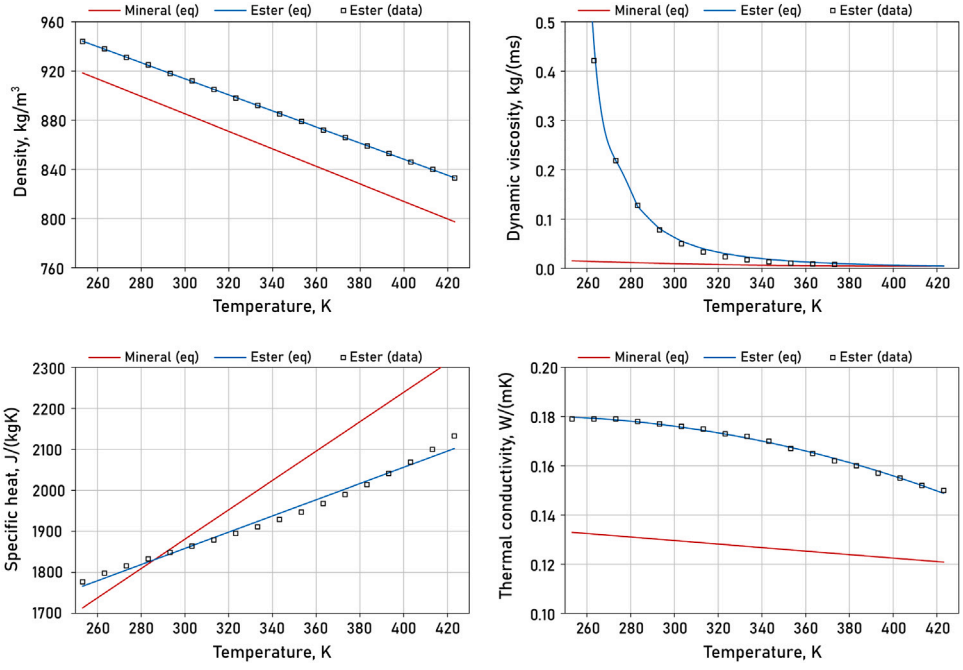

Fig. 7. Comparison of thermo-physical properties of mineral and ester oils.

3.7. EMAG boundary conditions

The EMAG model presented in this paper has three low and three high voltage coils. They are the source of magnetic potential. Additionally, because the magnetic field is conducted mainly by the core, magnetic vector potential boundary condition outside the transformer is assumed as equal to 0, as depicted in Fig. 8. The distance between the external boundary condition and the core was assumed as 10% of the total length/width. Because the 3-D model is computed for the half of the transformer, the face surface of the core, presented in Fig. 8, is set as tangential flux boundary condition. It ensures correct symmetry flux division.

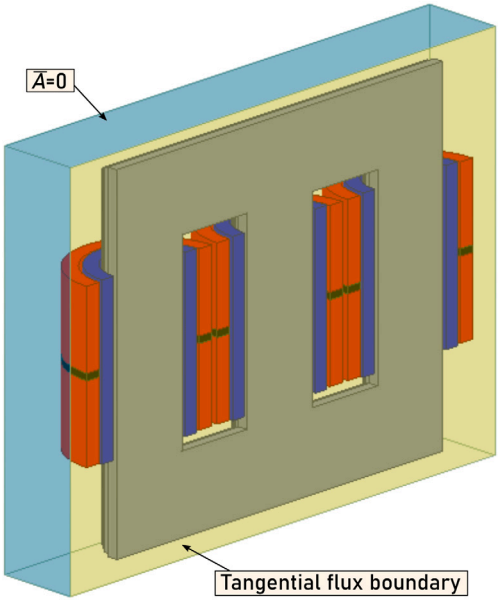

Fig. 8. Boundary conditions of the EMAG model with a zero magnetic vector at the boundaries of the domain (blue) and a tangential flux boundary being a symmetry of the domain (yellow). (For interpretation of the references to colour in this figure legend, the reader is referred to the web version of this article.)

3.8. CFD boundary conditions and the coupling between models

Numerous external and internal boundary conditions define the coupled CFD–CFD model presented in this paper. The external boundary conditions are used to describe the heat dissipation from the power transformer to the ambient, based on the climate data for each case investigated in this study. They are related only to the tank CFD model and to the supporting analytical model of radiators. Internal boundary conditions are defined for both CFD models. They are set at the interfaces between both CFD models and are used for the coupling between them.

This part of the paper describes all the aspects of the boundary conditions. Firstly, the investigated climate scenarios for which the simulations were performed are characterised, followed by the radiator analytical model results used as the input data for the tank CFD model. Then, each numerical model is described in terms of its external and internal boundary conditions. The coupling between both CFD models is discussed with a characterisation of all the corresponding boundary conditions employed for the coupling procedure. Description of all the boundary conditions is presented in Fig. 9. This scheme presents the organisation of the boundary conditions for both CFD models and the data transfer between them.

3.8.1. Investigated scenarios

The cases investigated in this study cover a variety of ambient conditions. They are related to cold and hot seasons in two different climate zones: the hot (Santa Fe, Argentina) and the moderate (Gliwice, Poland). Six different scenarios were compared based on the data from a climate database [39]. These are:

- the minimum monthly temperature in January in Gliwice (−5.8°C),
- the average monthly temperature in January in Gliwice (−1.4°C),
- the average monthly temperature in July in Santa Fe (12.2°C),
- the average monthly temperature in July in Gliwice (18.6°C),
- the average monthly temperature in January in Santa Fe (25.3°C),
- the maximum monthly temperature in January in Santa Fe. (32.0°C).

This temperature set appropriately represents the typical conditions for different seasons in both climate zones and excessively hot or cold long-term conditions in summer and winter.

Regarding boundary conditions, the ambient temperatures were set in the tank CFD model at the external tank walls. More importantly, the information about the ambient conditions was used to evaluate the mass flow rate and the temperature of the cooled oil using the reduced model of radiators. This aspect is described in detail in further Sections 3.8.2 and 3.8.4.

3.8.2. Radiators analytical model

As mentioned, radiators performance within the CFD part of this study is represented using a previously developed reduced model [25,26]. The model was adjusted to the geometry and capacity of the 8.5 MVA power transformer. The physical quantities determined using the reduced model are the flow rate of the oil flowing through a single radiator and the temperature of the cooled oil.

The results from the radiators reduced model are the input data for the tank CFD model are given in Table 5 for all the ambient conditions compared in this study for both oils. A detailed description of the boundary conditions that use these data is given in Section 3.8.4 dedicated to the tank CFD model.

3.8.3. Windings CFD model

The most significant group of boundary conditions defined for the windings CFD model is a set of pressure-type inlet and outlet boundary conditions located at the bottom and the top of this model domain, respectively. They are important because they guarantee the proper behaviour of the natural convection based on the buoyancy flow. Because the fluid domain includes vertical oil ducts that allow the oil to flow through the HV windings, LV windings, and through the narrow gap between the core limb and the windings, 5 inlet and 5 outlet boundary conditions are set in this model. Each represents an interface between both CFD models where the oil flows into and flows out the numerical domain of the particular CFD model. As mentioned before, pressure-type boundary conditions were used in the windings CFD model defined using the temperature and the total static pressure which is the sum of the reference pressure value equal for all the defined inlet and outlet conditions and the hydrostatic pressure being dependent on the localisation of each boundary. Due to the

Table 5
Boundary conditions in the CFD tank model obtained using the reduced radiator model.

		Ester oil		Mineral oil	
Case	t_{amb}, °C	t_{oil}, °C	VFR, ltr min^{-1}	t_{oil}, °C	VFR, ltr min^{-1}
WINTER MIN PL	−5.8	32.1	8.94	37.6	15.60
WINTER AVG PL	−1.4	37.7	9.54	42.6	15.90
WINTER AVG ARG	12.2	54.1	10.86	53.9	16.56
SUMMER AVG PL	18.6	62.4	12.48	65.2	17.16
SUMMER AVG ARG	25.3	70.9	14.34	72.8	17.52
SUMMER MAX ARG	32.0	75.0	15.30	80.3	17.88

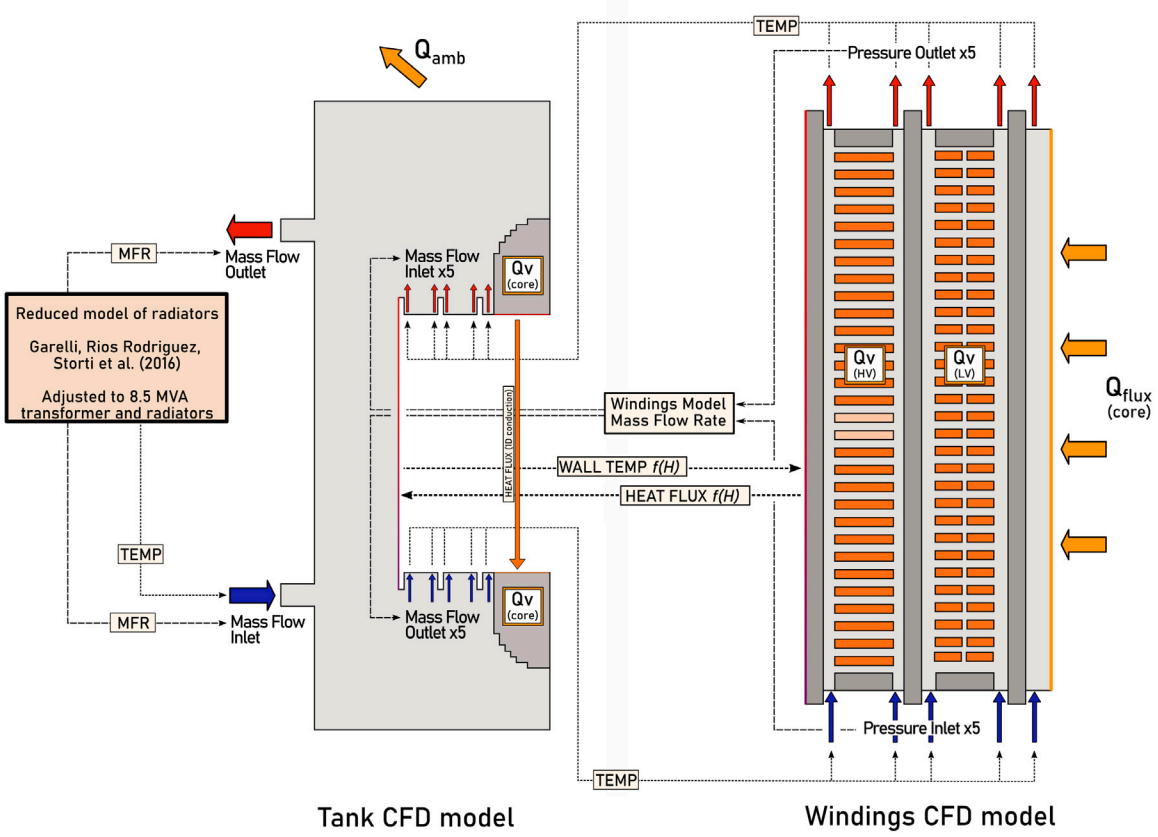

Fig. 9. A complete scheme of CFD models coupling using the corresponding boundary conditions.

natural convection phenomena, the buoyancy forces drive the oil flow within the windings, resulting in a certain mass flow rate of the oil at the boundary conditions. The information about the temperature at a particular inlet boundary condition results from CFD model coupling, described in Section 3.8.5.

As described in Section 3.2, the transformer core limbs were removed from the geometrical domain. However, they are represented by a cylindrical surface present in the windings CFD model. In order to provide the heat losses generated within the removed volume of the core, a wall-type boundary condition with a fixed heat flux was defined in the windings CFD model. In that way, the total heat that would be generated within the volume removed from the geometrical domain is balanced by the total heat provided by the heat flux defined at the proper surface with w known area.

In the power transformer, a minor heat generated within the HV windings is transferred by the external surface of the outer insulation tube of windings into the oil tank. This surface can be treated as an interface between the numerical domains of both CFD models. The corresponding surfaces in both models were coupled, as it is described in Section 3.8.5. In the windings CFD model, this surface was defined using a wall-type boundary condition with the 1-D distribution of the temperature along with this surface height.

3.8.4. Tank CFD model

In the tank CFD model, the data obtained with the analytical model of radiators were used to define the boundary conditions at the pipes connecting the transformer tank with the radiators, as can be observed in Fig. 9. The cooled oil flows into the transformer tank by the bottom pipe represented by the inlet boundary condition defined with a fixed temperature and the mass flow rate according to the data from Table 5. The top pipe is represented by the outlet boundary condition with a fixed mass flow rate as the same oil quantity flows from the transformer tank into the radiator. Considering that 1/4th of transformer interior is included in the computational domain of this CFD model, two pairs of inlet/outlet boundary conditions are defined to represent two out of eight radiators equipped to the power transformer.

Regarding the external boundary conditions, the effect of the heat dissipation from the outer surfaces of the transformer tank to the ambient is considered as well. It covers both the convective and radiative heat transfer to the ambient. The convective heat transfer is defined based on the empirical correlations for the dimensionless Nusselt number (Nu) available in the literature: by Churchill and Chu [40] for the vertical sidewalls, and by Lloyd and Morgan [41] for the horizontal top wall. These formulas are given in Eqs. (14) and (15), respectively. In these equations, the Prandtl (Pr), Rayleigh (Ra), and Grashof (Gr) dimensionless numbers are also present, defined in Eqs. (16)–(18). Thermo-physical properties in this formulation were evaluated for the air taking the average temperature of the boundary layer: $(T_{sur}+T_{amb})/2$ [42].

$$\mathrm{Nu} = 0.68 + \frac{0.67\,\mathrm{Ra}^{1/4}}{\left[1 + (0.492/\mathrm{Pr})^{9/16}\right]^{4/9}} \tag{14}$$

$$\mathrm{Nu} = 0.59\,\mathrm{Ra}^{1.4} \tag{15}$$

$$\mathrm{Ra} = \mathrm{Gr}\,\mathrm{Pr} \tag{16}$$

$$\mathrm{Pr} = c_p\,\mu/k \tag{17}$$

$$\mathrm{Gr} = g\,\beta\,L^3\left(T_{sur} - T_{amb}\right)/\nu^2 \tag{18}$$

where β is the coefficient of thermal expansion, L is the characteristic length for the particular correlation, T_{sur} is the local surface temperature, T_{amb} is the ambient temperature, and ν is the kinematic viscosity.

The convective heat transfer coefficient is evaluated based on the Nusselt number as given in Eq. (19), and the convective heat flux

based on Newton's law (Eq. (20)). The radiative heat flux is defined in Eq. (21) [42]. Finally, the total heat flux is a sum of these two mechanisms (Eq. (22)).

$$h_{conv} = \mathrm{Nu}\frac{k}{L} \tag{19}$$

$$q_{conv} = h_{conv}\left(T_{sur} - T_{amb}\right) \tag{20}$$

$$q_{rad} = \sigma_r \varepsilon \left(T_{sur}^4 - T_{amb}^4\right) \tag{21}$$

$$q = q_{conv} + q_{rad} \tag{22}$$

where h_{conv} is the convective heat transfer coefficient, q_{conv} is the convective heat flux, q_{rad} is the radiative heat flux, σ_r is the Stefan–Boltzmann constant (5.67e−8 W m^{-2} K^{-4}), ε is the emissivity of the outer casing surface, and q is the total heat flux at the outer surface.

In Section 3.8.3, the internal boundary conditions defined on the interfaces between both CFD models were discussed. To model oil flow through the windings, the appropriate inlet and outlet boundary conditions are defined in the tank CFD model in the regions where the oil flows into the windings and flows out of them. At the bottom of the windings, a set of outlet boundary conditions was defined. Analogously at the top of the windings, the inlet boundary conditions were defined. Every inlet-type boundary condition in one CFD model has the corresponding outlet-type boundary condition in the second CFD model. In the tank CFD model, the oil mass flow rate at every inlet and the outlet boundary condition results from the oil mass flow rate determined using the windings CFD model. The inlet-type boundary conditions at the top of the windings must be defined using the oil temperature. That quantity is evaluated as a result of the CFD–CFD coupling, described in the following section.

As discussed before, the outer insulation tube surface is another interface between both CFD models used in the coupling procedure. In the tank CFD model, that surface is defined using a wall-type boundary condition with the temperature distribution defined along with this surface height.

The last aspect regarding the internal boundary conditions defined in the tank CFD model is related to the temperature difference between the top and the bottom yoke. The top yoke is expected to have a slightly higher temperature than the bottom one. The heat transfer between these parts of the magnetic core cannot be solved implicitly in any of CFD models because the core limbs were removed from the domain of both models. Because of that, a 1-D heat conduction equation was defined based on Fourier's law to transfer the heat from the top yoke to the bottom one between the surfaces used to close the domain of the tank model within the core region. These heat fluxes are defined at the surfaces as given in Eq. (23) with the positive value for the bottom surface and the negative value for the top surface. In that equation, the thermal conductivity was set as 48.8 W m^{-1} K^{-1} according to the material data for the core given in Table 2.

$$q = k\frac{\Delta T}{l} \tag{23}$$

where ΔT is the temperature difference between the surfaces being the boundary conditions and l is the distance between them.

3.8.5. CFD-CFD models coupling

The coupling of the windings and the tank CFD models is realised using the pairs of the adequate internal boundary conditions. Fig. 9 which presented all the boundary conditions of both CFD models also includes the flowchart of the data transferred between the models. Physical data exchanged between the models are:

- The mass flow rate and the cooled oil temperature predefined using the input data given in Table 5.
- The mass flow rate of the oil flowing through the windings defined at the oil–oil interfaces between both models. Its value is determined using the windings CFD model. It is worth mention that due to both vertical and horizontal flow, the oil mixes within each part of the windings. As a result, the mass flow rate balance between the two ducts of each part may not be the same at its inlet and outlet section. It should be pointed out that the CFD windings model covers 1/16th of one phase coil. Therefore, the mass flow rate is appropriately adjusted to the tank model domain covering half of the side coil and a quarter of the middle coil.
- The temperature of the oil at the same boundary conditions is exchanged in the same manner. The oil temperature at the top boundary conditions is transferred from the windings model to the tank model. Similarly, the oil temperature at the bottom boundary conditions is transferred from the tank model to the windings model during the iterative process described in Section 3.4.
- The outer surfaces of the insulating tubes are present in both CFD models. The oil does not flow through them, but these surfaces transfer some minor portion of the heat generated within the HV windings to the oil present in the transformer tank. For that reason, the corresponding boundary conditions at the outer insulating tube surfaces were coupled as well. As mentioned before, that surface was defined using a temperature distribution in the windings CFD model and using the heat flux distribution in the tank CFD model. The distribution is 1-D being the function of the surface height.

4. Results and discussion

4.1. Energy losses estimation

As discussed in Section 3.2, different formulations of the EMAG model numerical domain were introduced to develop an accurate and

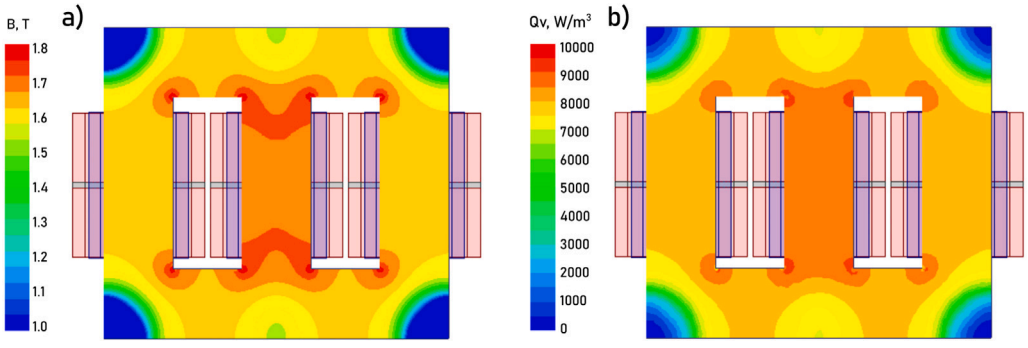

Fig. 10. Distribution of (a) the magnetic flux density in T and (b) the heat sources in W/m^3 in the core for the scenario with constant temperatures given by the manufacturer.

efficient model for the power losses evaluation. To assess the effect of geometrical simplifications, i.e., windings homogenisation and the domain dimensionality reduction, the total losses were compared for the reference temperatures (70°C for the core, 78.5°C for the HV windings, and 71.7°C for the LV windings) as shown in Table 6. According to the results, the windings losses obtained from both 2-D models were at the same level, therefore this simplification was confirmed to be appropriate. However, the second geometrical simplification, i.e., the geometrical domain dimensionality reduction from 3-D to 2-D, affected the core losses. For that reason, the 3-D domain with fully homogenised windings was selected as the final one to evaluate the spatial distribution of the volumetric heat sources within the windings and the core.

The most important advantage of using the EMAG model is the possibility to obtain a detailed distribution of the volumetric heat sources within the windings and the core. Fig. 10(a) presents the distribution of the magnetic flux density within the cross-section of the core for the constant temperature of 70°C. The highest magnetic flux density is observed in the central column of the core because magnetic flux is a superposition of these from the first and third columns. Because magnetic circuits are closed by the shortest paths, the magnetic flux density is also higher at right-angle and sharp corners. The relation between the magnetic flux density and the volumetric heat sources is given by Eq. (6), and its distribution is depicted in Fig. 10(b). The highest volumetric heat source is again observed in the central column and sharp corners, following the magnetic flux.

The EMAG model results presented above refer to a scenario with constant temperatures of the core, the LV, and the HV windings. That scenario can be treated as a reference state. As discussed in Section 3.6, the $P = P(B)$ characteristics of the core are dependent on the temperature distribution. Thus core losses are dependent on the temperature as well. Similarly, the electric conductivity of copper in the windings is dependent on the temperature. Therefore, according to Eqs. (1)–(2), ohmic losses are also dependent on the temperature. As discussed in Section 3.4, the influence of the temperature on the volumetric heat losses was included in both CFD models in the source term formulation of the energy equation. The linear relationship was considered as +0.37%/K for the windings and −0.15%/K for the core regarding the temperature rise above the reference state computed using the EMAG model.

For that reason, for each scenario analysed in this paper, the total amount of losses is different due to different temperatures in the core and windings. Fig. 11 presents the total losses for all the scenarios analysed in this paper compared with the reference losses discussed previously.

As seen, most of the heat is generated within the HV part of the windings. The amount of heat generated within the LV windings is approximately 30% lower. Considering the total heat generated within the entire transformer, the ohmic losses are responsible for almost 90% of the total heat generated within the power transformer. It suggests that the cooling of windings is of particular importance to guarantee the safe operation of that device. Consequently, the total amount of the heat generated within the transformer rises with the ambient temperature increase according to the assumed relationship between windings temperature and the ohmic losses change. The difference between the heat generated for the highest and the lowest ambient temperatures of 32.0°C and −5.8°C is approximately 5.6 kW. Such a difference affects the transformer hotspot temperatures not significantly. The cooling oil type affects the temperature level of windings and the core, which will be discussed in Section 4.3; however, it does not significantly affect the generation of losses.

Table 6
Power losses from the EMAG models with different computational domains.

	Core losses, kW	Windings losses, kW	Total losses, kW
2-D fully homogenised	5.65	40.35	46.00
2-D disks homogenised	5.65	40.35	46.00
3-D fully homogenised	5.43	41.01	46.44

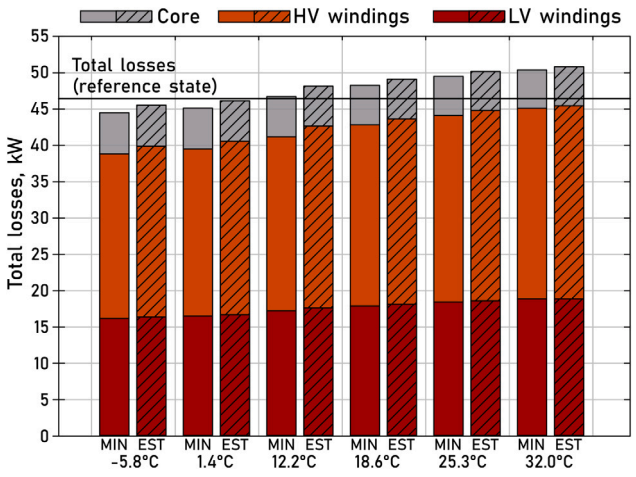

Fig. 11. Total losses in kW generated within the core and the windings of the power transformer for all the analysed cases.

4.2. Fluid flow distribution

The efficient cooling of the magnetic core and more important, of the windings depends on the oil flow within these regions. In ONAN-type transformers, the oil flow is driven by buoyancy forces. On the other hand, the friction of the viscous oil acts as a resistance to the natural flow of the cooling oil. In order to assess the oil flow through the transformer active parts globally, the oil mass flow rate (MFR) through the gap between the core and the windings and through the ducts of the LV and HV parts was compared in Fig. 12. This characteristic is focused on comparing the mineral oil and more viscous ester oil flow in different transformer operating conditions in terms of the ambient temperature.

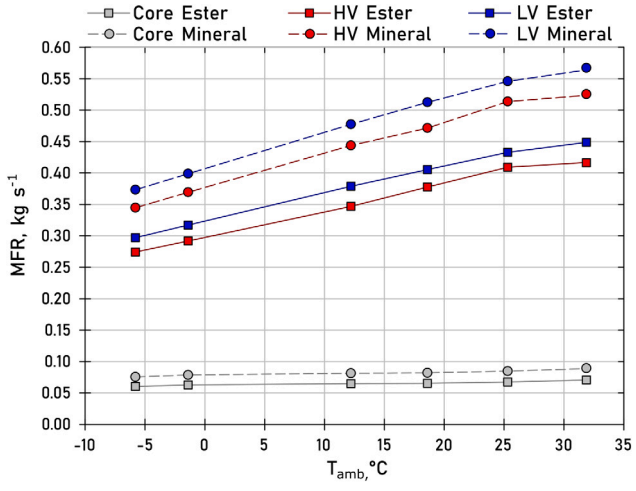

Fig. 12. Mass flow rate in kg s^{-1} of the oil flowing through the ducts of the LV and HV windings and the gap between the core and the windings a function of the ambient temperature for all the investigated cases.

In general, the mass flow rate of the oil flowing through the gap between the core and the windings is approximately 0.065 kg s^{-1} and 0.082 kg s^{-1} for the mineral and ester oils, respectively. Within the analysed range of the operating conditions, the flow rate is relatively constant. Such behaviour is a result of the simple path of the oil flow. Therefore, the friction being an effect of the oil viscosity is not as

significant. Also, the amount of heat dissipated from the core, which drives the buoyancy force, is relatively low. Consequently, the mass flow rate of the oil in that gap is minor.

In the case of the flow along both parts of the windings, an effect on the oil properties is noticeable. First of all, depending on the operating conditions, the mass flow rate of the oil through the HV windings is in the range of 0.27 kg s^{-1} to 0.42 kg s^{-1} for the ester oil and 0.34 kg s^{-1} to 0.53 kg^{-1} for the mineral oil. In the case of the LV windings, the mass flow rate is slightly higher, namely 0.30–0.45 kg s^{-1} and 0.37–0.57 kg s^{-1} for the ester and mineral oil, respectively. Again, it is seen that the mass flow rate of the ester oil is lower than that of the mineral oil due to the higher viscosity. It is worth mention that more oil flows through the ducts of the LV windings. It is a result of the presence of an additional vertical oil duct because of a separated configuration of that winding as discussed in detail in Sections 2 and 3.2.

An analysis of the local velocities is described to present the oil flow behaviour through the windings in detail. In disk-type windings, a horizontal flow of the oil in the gaps between disks plays a significant role in effective heat dissipation. As mentioned in Section 2, the analysed transformer is not equipped with the washers. Therefore, the horizontal flow of the oil is not directed. As discussed before, in the LV part, each disk is split; thus, the horizontal oil flow is slightly enhanced. To discuss the horizontal oil flow between the disks, the horizontal velocity components are presented in Fig. 13(a) across the vertical cross-sections of the windings for the selected cases. These cross-sections, shown in Fig. 13(b) were set in the middle of vertical oil gaps in HV windings and two parts of LV windings separated by an additional duct. The positive velocity values refer to the oil flow away from the core to identify the oil flow direction.

As seen in the figure, the oil flow within the LV windings is more effective. Excluding the regions near the top and bottom of the windings, the horizontal velocities in LV windings reach approximately 1.2 mm s^{-1} for the mineral oil, and the flow behaviour mimics the zig-zag flow, primarily seen for the hottest ambient conditions, e.g., in the region between 35th and 40th LV disk. In the ester oil flow, the horizontal velocities do not exceed 0.5 mm s^{-1}, which may be considered rather stagnant.

The velocities are significantly lower within the HV windings reaching up to 0.4 mm s^{-1} for the mineral oil in the hottest ambient conditions. It can be concluded that this kind of configuration of windings, namely non-separated disks without the presence of washers, leads to oil flow stagnation.

To discuss the oil flow phenomena between the disks in detail, it is worth comparing the local velocity vectors for both oils as presented in Fig. 14 for the cases represented by the highest ambient conditions, where the differences are the most significant. According to the colour scale, the oil velocities are remarkably higher within the vertical oil ducts. What should be underlined is the change of the flow direction within the LV part for the mineral oil between disks 35–40 as presented previously in Fig. 13. The change of the velocity magnitudes in the middle and side oil ducts proves that this phenomenon affects the oil flow behaviour within the LV windings. Moreover, the local changes of the flow direction within the oil gaps in HV and LV parts for both oils prove that the flow is not purely laminar and local eddies are present within the windings of the power transformer.

The coupled numerical model of the power transformer presented in this study allows for determining the oil flow characteristics within the interior of the power transformer tank. Fig. 15(a) and (b) present the velocity vectors in selected vertical and horizontal planes inside the transformer tank and along the numerical domain symmetry planes for the mineral and ester oils, respectively. This comparison is made for the ambient temperature of −5.8°C, where the most significant differences are expected for the mineral and ester oils due to the different oil flow rates through the radiators, computed using the reduced model of radiators. Two vertical planes (called V1 and V2) and two horizontal planes (called H1 and H3) were set along the oil pipes connecting the transformer tank with radiators, and one additional horizontal plane H2 was set near the upper side of the windings, as shown in Fig. 15(c). The used colour scale is in the range of 0 to 30 mm s^{-1}. However, the upper bound marked with red colour also represents the velocity values exceeding 30 mm s^{-1}, because such a high velocity occurs only near the oil pipes where a detailed comparison of the flow is not significant.

For both cases, the velocities of the oil flowing out of the bottom pipes exceed 30 mm s^{-1}; however, in the mineral oil, the flow rate is higher according to Table 5. For that reason, the oil flows out the bottom pipes more intensively in the case of the mineral oil. In the case of the ester oil, there is a slightly different flow character, where the oil flows up after entering the transformer tank. For both cases, the oil velocity is very low in the bottom region of the tank below the windings. It is a region where the circulation is not seen, and the cooled oil may be heated only due to heat generated in the bottom yoke. Above that area, namely in the region between planes H1 and H2, the fluid circulation is more intensive in the mineral oil case where the values of velocity reach 9 mm s^{-1}. It can be a result of a higher rate of cold oil flowing out of the radiator. The fluid flow becomes more intensive in the top region of the transformer tank, at the level of the H3 plane. At that position, the velocity values are in the range of 6 to 20 mm s^{-1}

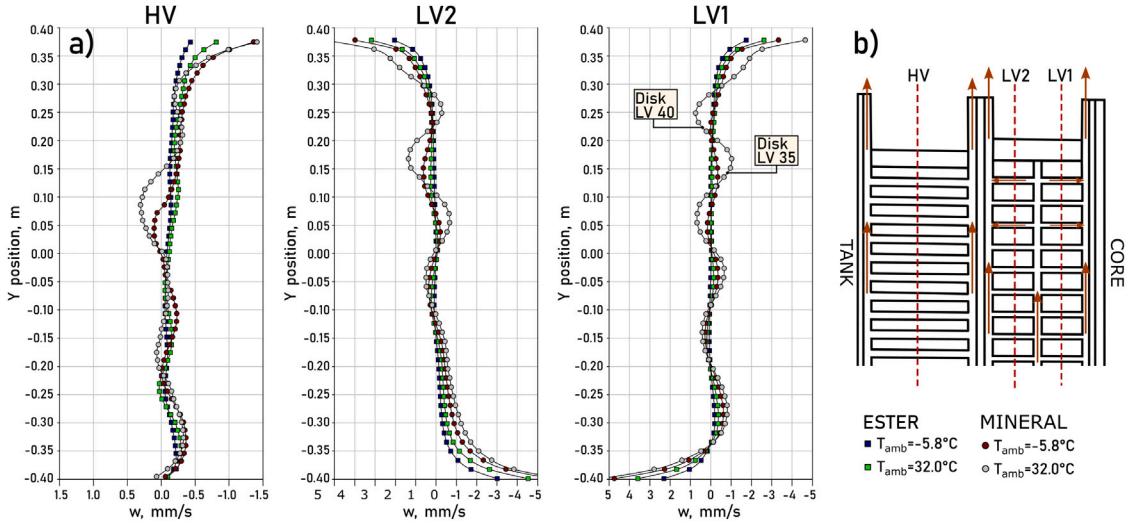

Fig. 13. (a) Average horizontal oil velocities in mm s^{-1} between the disks within the characteristic cross-sections HV, LV2, LV1 for the mineral and ester oils under the ambient temperatures of −5.8°C and 32.0°C and (b) scheme presenting the location of the HV, LV2 and LV1 cross-sections.

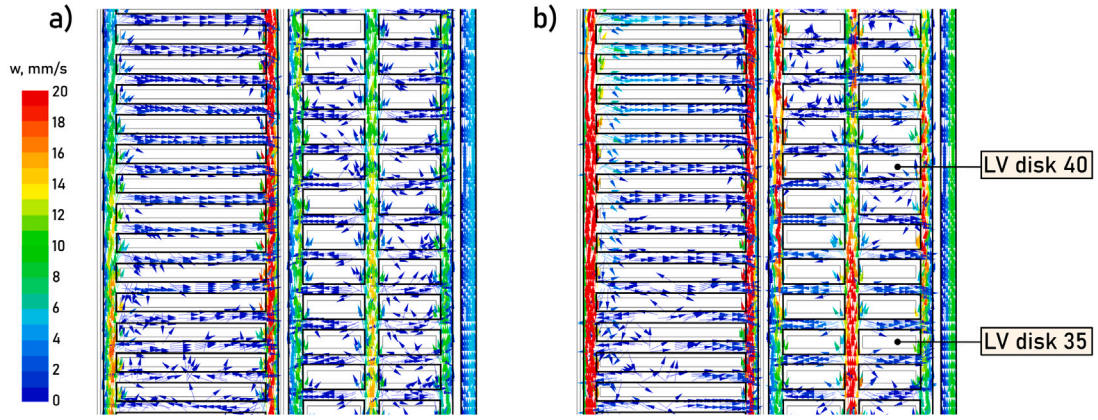

Fig. 14. Vectors coloured in the velocity scale in mm s^{-1} presenting (a) the ester oil and (b) the mineral oil flow direction within the windings for the highest ambient temperature (32.0°C) in the region of 35–40 LV disk. (For interpretation of the references to colour in this figure legend, the reader is referred to the web version of this article.)

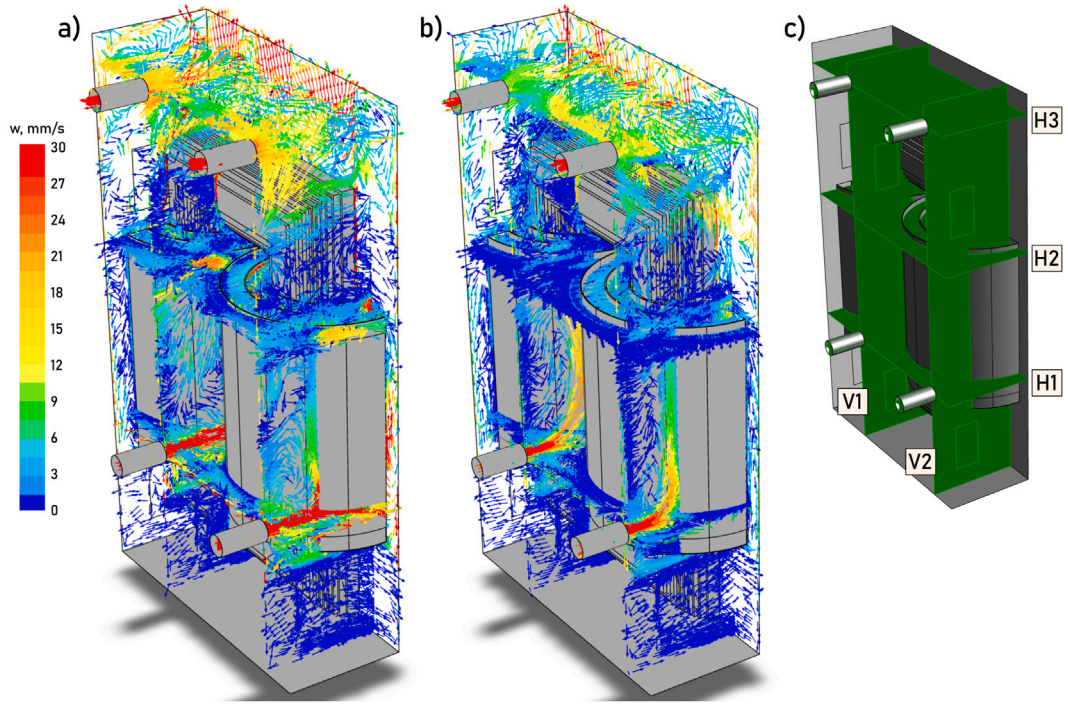

Fig. 15. Vectors coloured in the velocity scale in mm s^{-1} presenting the oil flow within the transformer tank in planes V1, V2, H1, H2, H3 for ambient temperature of −5.8°C for (a) the mineral oil and (b) the ester oil together with (c) the localisation of the planes. (For interpretation of the references to colour in this figure legend, the reader is referred to the web version of this article.)

and 3 to 15 mm s^{-1} for the mineral and ester oils, respectively. For both cases, a convective flow is seen above the top yoke of the transformer, where the velocity values exceed 18 mm s^{-1} and 30 mm s^{-1} locally.

4.3. Temperature fields in windings

A detailed analysis of temperature fields within the power transformer is an important aspect to assess its performance and the capability of cooling in the ONAN regime by using mineral or ester oils. Fig. 16(a) and (b) present the temperature fields within the cross-section of windings cooled by the mineral and the ester oils, respectively. The comparison was performed for the ambient temperature of 32.0°C, which is the case that results in the highest temperatures within the transformer and the same one that the velocity vectors were presented in Fig. 14. Comparing the temperature fields for both oils shows that the windings are cooled more effectively with the mineral oil. The difference is seen especially in the HV part. The temperature of most HV disks is more uniform in the case of mineral oil. In the case of the ester oil, the differences in temperature of different disks are significant. It is due to a worse oil circulation through the horizontal oil ducts, as discussed in Section 4.2. At the level of the HV disk 13, a local HST is seen with the temperature reaching 113°C. However, the hottest disk is the HV disk 47 with the maximum temperature of 117.6°C. At a similar position in the mineral oil case, a local HST is noted at the HV disk 45 with the temperature reaching only 105.5°C. It is worth noting that in the case of mineral oil, the last HV disk is the hottest one with a temperature of 108.7°C. The cooling of that disk is less effective because its top side is not cooled with the oil but is covered by the supporting plate.

The effect of two inactive disks is also seen. The HV disks 29 and 30 have approximately 10–15 K lower temperatures than the other disks for both compared cases. In the case of LV windings, the temperature level is significantly lower. Firstly, less heat is generated in that part, and secondly, the oil circulation is more effective due to the additional

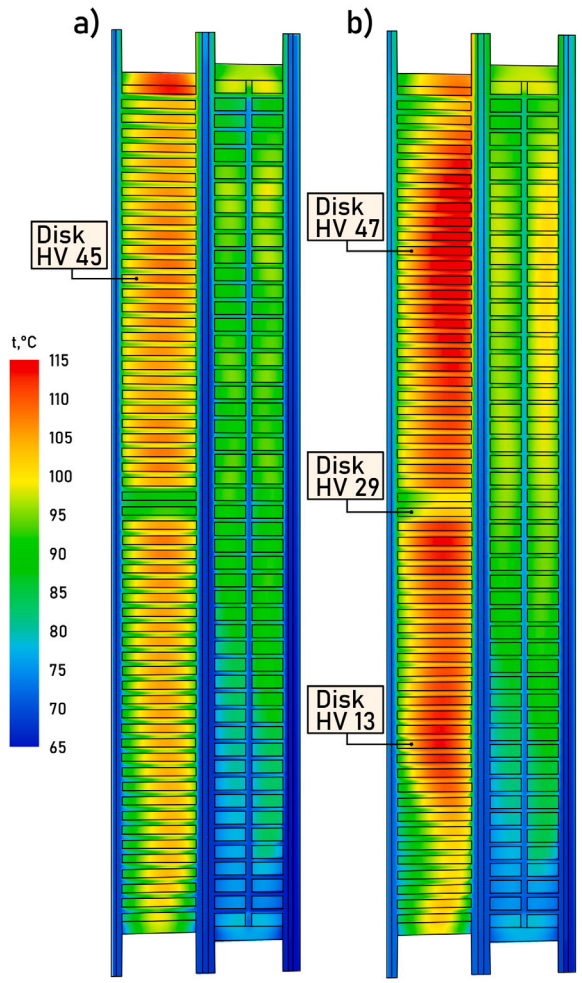

Fig. 16. Temperature field in °C in the cross-section of windings for cases with (a) the mineral and (b) the ester oils working in the ambient temperature of 32.0°C.

vertical oil duct. Most LV disk temperatures were approximately 90 to 95°C for both oils.

4.4. Average temperatures

One of the most common thermal indicators of transformer performance is the average temperature of the windings and core. Fig. 17 presents the comparison of these temperatures for all the scenarios considered in this study for both oils. As seen, the LV and HV windings temperatures are higher if the ester oil is used as a cooling medium. The higher the ambient temperature and the oil temperature, the smaller the windings temperature difference between two oils used in the same ambient conditions. It is due to the viscosity of Midel eN 1204 ester oil, which is higher than the mineral oil viscosity, especially at low temperatures. The exception is seen for the case with the ambient temperature of 32.0°C in the LV part. The windings temperature is almost equal and does not depend on the oil type. In this case, the viscosity of the ester oil was not significantly higher than the mineral oil. Moreover, the additional oil duct in the LV windings allowed for an effective cooling oil flow. In the case of the highest ambient temperature of 32.0°C and the mineral oil, the windings average temperature reaches 100.5°C and 91.8°C for the HV and LV windings, respectively. For the same temperature but the ester oil, the windings average temperature reaches 104.8°C and 91.7°C for HV and LV windings, respectively. In general, the differences in the average temperatures of HV windings are apparent but not crucial for both oils.

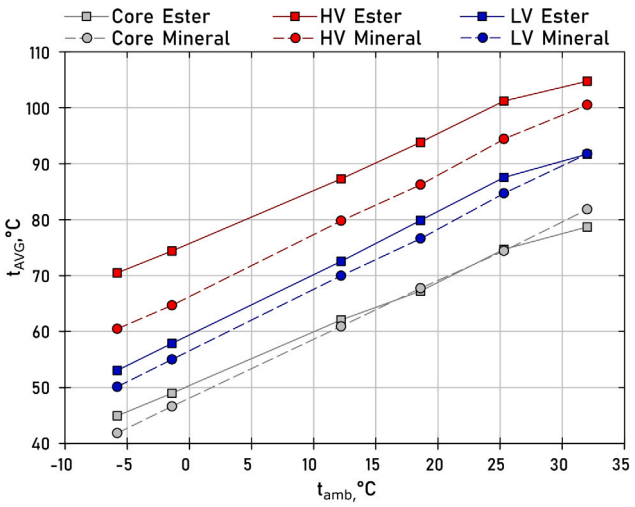

Fig. 17. The average temperature of the core, HV and LV windings in °C for all the investigated cases.

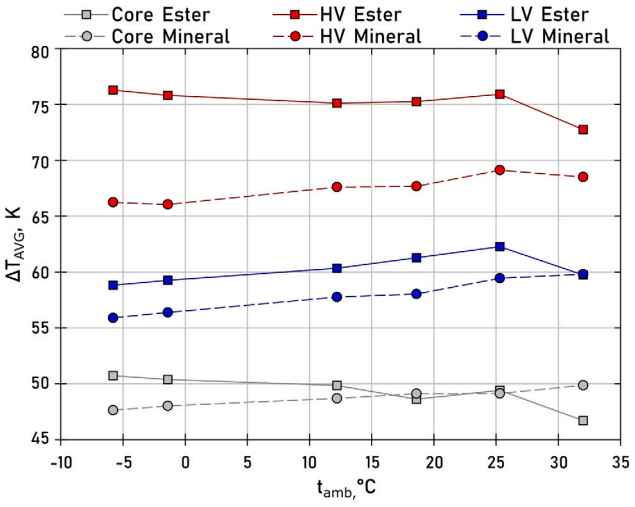

Fig. 18. The average temperature of the core, HV and LV windings expressed in K as a temperature rise above the ambient temperature for all the investigated cases.

The average temperature of the core parts present in the numerical domain, namely the top and bottom yokes, was compared. In general, the average temperature of the core does not depend on the oil type significantly. For the coldest conditions, the yokes average temperature was 41.8°C and 44.9°C for the mineral and ester oils, respectively. For the moderate ambient conditions between 18.6°C and 25.3°C, the average yokes temperature was almost equal for both oils. Furthermore, for the hottest ambient temperature, the yokes temperature was 89.2°C in case the mineral oil and 78.7°C when the ester oil was used, which is an opposite relation to the cases with the low ambient temperature.

The temperature level in the electrical devices is very often expressed as the temperature rise above the ambient as $\Delta T = t - t_{amb}$. Fig. 18 presents the same results as previously in Fig. 17 but expressed as the temperature rise above the ambient conditions. For the ester oil cases, the HV windings temperature rises by approximately 75 K above the ambient temperature, depending on the case. The LV windings temperature increases by approximately 60 K. It can be noticed that in the case of the ester oil and the ambient temperature of 32.0°C, the temperature rise is significantly lower. The reason was already discussed in the previous paragraph. For the mineral oil, the winding temperature rise is slightly lower than for the ester oil. Namely, the

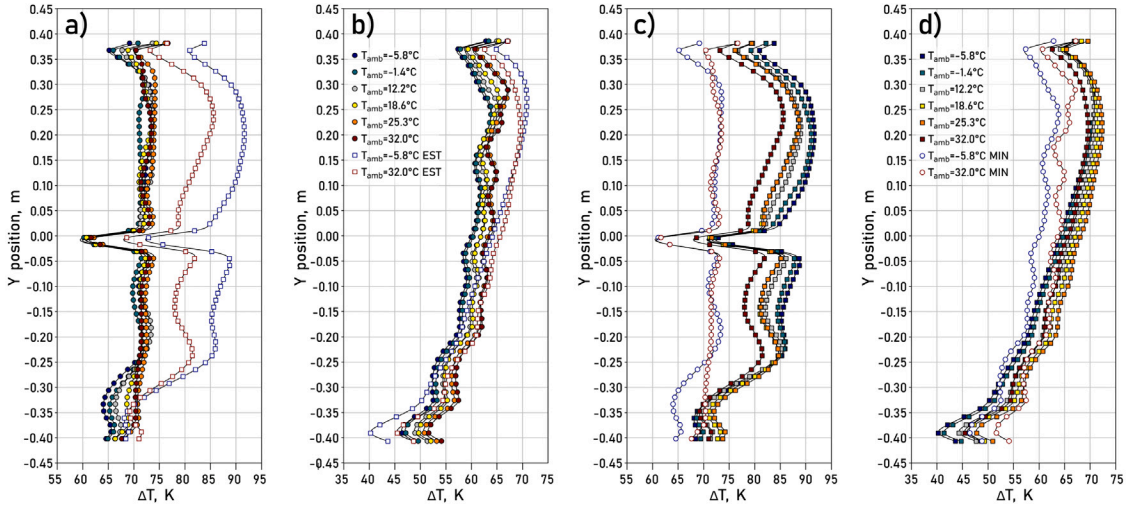

Fig. 19. The maximum temperatures for all the investigated conditions expressed in *K* as a temperature rise above the ambient temperature in (a) HV disks for the mineral oil (b) LV disks for the mineral oil, (c) HV disks for the ester oil and (d) LV disks for the ester oil.

mean values of the windings average temperature rises are approximately 67 K and 57 K for the HV and LV parts, respectively. The yokes average temperature rise for the mineral oil was 48 K to 50 K. For the ester oil, the yokes average temperature rise was from 46 K to 51 K for all the ambient conditions and was lower for higher ambient temperatures. It can be mostly a result of a significant change of the oil flow rate through radiators compared in Table 5. For the cold ambient conditions, the cooled oil flow was lower; therefore, the circulation of the oil within the tank was lower and resulted in less effective cooling of the yokes.

4.5. Hotspot temperatures

The lifetime expectancy of the power transformers depends on the HST in its most extremely heated parts. According to the temperature fields presented in Fig. 16, the temperature distribution within the windings is not uniform, especially in the HV part of the investigated unit. Therefore, a detailed assessment of the maximum temperature rises in the individual HV and LV disks related to the ambient temperature was performed for all the conditions. Fig. 19(a) and (b) present the maximum temperature of each HV and LV disk, respectively, for all the conditions being compared for the mineral oil, while Fig. 19(c) and (d) refer to the same data for the ester oil. For the convenience of results interpretation, each graph also includes the second oil results for the coldest and hottest ambient conditions being analysed.

It is shown in Fig. 19(a) that in the case of the HV windings, the temperature is fairly uniform in all disks cooled by mineral oil. There is no significant variability in the level of the temperature rise for different ambient conditions. For the case with the ester oil cooling, the character of the maximum local distribution in HV disks is different as presented in Fig. 19(c). Two regions with a higher level of temperature rise can be seen, i.e., below two inactive disks 29 and 39 and above them. For the ester oil, the lower oil circulation effect is significant, resulting in a higher temperature rise in HV windings.

In the case of LV disks, the maximum temperature rises are presented in Fig. 19(b) and (d) for the mineral and ester oils, respectively. As seen, the maximum temperature level for both oils is rather uniform in disks but higher in the upper disks due to higher oil temperature.

In the case of the mineral oil cooling, the effect of the oil circulation in different directions (zig-zag flow) is seen in Fig. 19(b) as the slightly disordered shape of the temperature characteristics. It is the effect of horizontal flow presented previously in Fig. 13 for cross-sections LV2

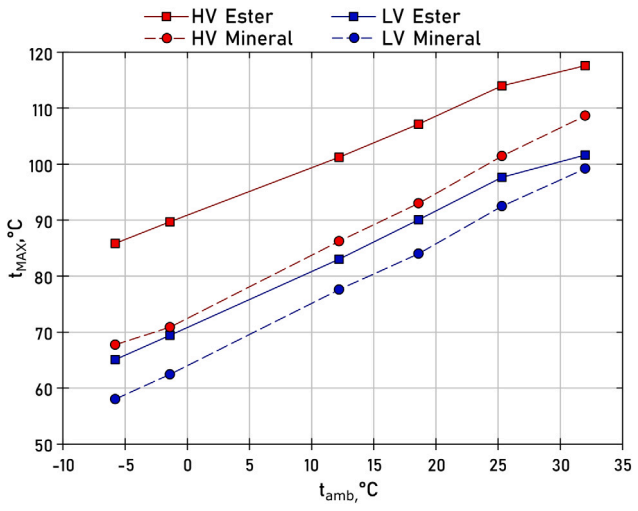

Fig. 20. The hotspot temperature of HV and LV windings in °C for all the investigated cases.

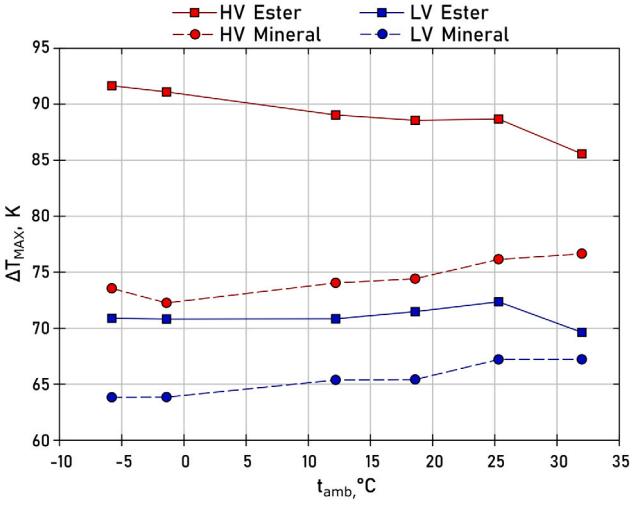

Fig. 21. The hotspot temperature of HV and LV windings expressed in *K* as a temperature rise above the ambient temperature for all the investigated cases.

and LV1. For the ester oil, that characteristic shown in Fig. 19(d) is rather smooth, which is a consequence of mainly vertical flow of the oil. The dependency of the ambient temperature is minor, especially for the mineral oil.

For a general assessment, the HST in the transformer windings, the global HST values are presented in Fig. 20. As discussed before, using the ester oil results in higher temperatures of the transformer windings, especially in the HV part. In the case of the ambient temperature of 32°C, the windings reach HST of 117.6°C. In the same ambient conditions, the HST of the HV part reaches a significantly lower temperature of 108.7°C. It is worth mentioning that the HV windings cooled by the ester oil reach that HST level at the ambient conditions of approximately 20°C. These numbers suggest that replacing the mineral oil with the ester oil may result in faster degradation of the insulating materials. In the case of LV windings, the difference in mineral and ester oil cooling is not as significant. For the highest ambient temperature, the HST of the LV disks reaches 99.2°C and 101.6°C in the case of mineral and ester oils, respectively.

The same HST values are expressed as a temperature rise above the ambient conditions in Fig. 21. In the mineral oil case, the average temperature rise for all the conditions is approximately 74 K and 65 K for the HV and LV windings, respectively. However, these values are not significantly dependent on the ambient conditions and consequently the oil temperature. Therefore, it can be concluded that the analysed unit is cooled by the mineral oil well at different climate conditions.

In the case of the ester oil, HST is higher in both parts of windings. In the LV part, the temperature rise is approximately 71 K and does not significantly depend on the ambient conditions. In the HV part, the HST temperature rise reaches almost 92 K in case of the winter conditions and the ambient temperature of −5.8°C. The temperature rise is lower in higher ambient temperature. In the case of the hot ambient temperature of 32°C, the temperature rise is approximately 86 K. It suggests that the cold oil viscosity significantly affects the cooling performance of the ester oil in the analysed unit where the oil flow through the gaps between disks is neither forced nor directed.

5. Conclusions

In this paper, a numerical study of the power transformer cooling with conventional mineral and biodegradable ester oils was performed for various ambient conditions related to hot and moderate climate zones characteristic to Argentina and Poland. The main difference in the oil properties is related to the significantly higher viscosity of the ester oil, especially at relatively low temperatures of the fluid.

Numerical models were prepared based upon technical documentation received from Tadeo Czerweny S.A., the manufacturer of the unit. The disk-type power transformer has a rated power of 8.5 MVA. The cooling is realised in the ONAN regime and involves 8 radiators.

Several approaches for EMAG model formulation were tested, and the final 3-D domain was simplified by homogenisation of disks into homogeneous cylinders. The results of total losses computed and those given by Tadeo Czerweny S.A. are in good agreement. The discrepancy is equal to about 0.1% at reference temperatures of 78.5, 71.7, and 70°C for HV windings, LV windings, and core, respectively, in the case of a 3-D fully homogenised model.

Separate CFD models were developed for characteristic parts of the transformer to perform the simulations efficiently. The first model was prepared for a detailed simulation of the oil flow within a complex structure of oil ducts in the windings. This 3-D model was reduced to a repeatable segment covering 1/16th of one-phase windings. The second 3-D CFD model was prepared to simulate the oil flow within 1/4th of the transformer tank. The numerical domain of this model included the oil domain and also the top and bottom yokes. The area of windings was excluded from this model. The performance of radiators was represented using the reduced model developed for a similar unit adjusted to the 8.5 MVA power transformer investigated in this paper.

An advanced EMAG–CFD–CFD coupling procedure was proposed to develop a complex and detailed but efficient simulation process, significantly reducing computational time. The EMAG model was used to generate the volumetric heat losses within the core and windings, followed by CFD computations. The two CFD models were coupled by using the characteristic boundary conditions. Simultaneously proceeded simulations permitted to obtain a converged solution allowing to characterise a detailed thermal state of the power transformer working at different conditions.

The fluid flow and the temperature fields were compared for different power transformer operating conditions when cooled by two different oils. The hotspot temperatures were identified in the low voltage and high voltage windings. According to the results, changing the mineral oil with the ester oil increased the maximum temperatures occurring in the windings, especially in the HV part. The reason for that is the less intensive oil circulation in the horizontal ducts between each HV disk. In the case of the LV windings, the difference was not as significant. In the hottest considered ambient temperature of 32°C, the maximum temperature in the HV windings increased from approximately 108°C to 118°C when the ester oil was used. In the case of LV windings, the hotspot temperature increased from approximately 99°C to 103°C.

It should be pointed out that the significant temperature rise was an effect of the lower ester oil flow through the radiators due to higher friction, relatively simple construction of HV windings without the washers or additional oil ducts, and the reduced oil circulation through the windings due to higher viscosity of ester oil.

In summary, the biodegradable ester oils can be successfully used as cooling and insulating fluids in the power transformers. In some cases, simple modifications in the configuration should be undertaken to provide better flow of the oil, e.g., using the washers to force a zigzag oil flow, creating additional vertical oil ducts within the windings or changing the construction of the radiators to minimise friction, which reduces the oil flow through the radiators.

CRediT authorship contribution statement

Michal Stebel: Conceptualization, Methodology, Formal analysis, Investigation, Writing – original draft, Visualization. **Krzysztof Kubiczek:** Methodology, Investigation, Writing – original draft, Visualization. **Gustavo Rios Rodriguez:** Methodology, Investigation, Resources, Writing – review & editing. **Michal Palacz:** Writing – review & editing. **Luciano Garelli:** Methodology, Investigation, Resources, Writing – review & editing. **Bartlomiej Melka:** Writing – review & editing. **Michal Haida:** Writing – review & editing. **Jakub Bodys:** Writing – review & editing. **Andrzej J. Nowak:** Writing – review & editing. **Pawel Lasek:** Investigation. **Mariusz Stepien:** Supervision. **Francisco Pessolani:** Resources. **Mauro Amadei:** Resources. **Daniel Granata:** Resources. **Mario Storti:** Resources, Supervision, Project administration. **Jacek Smolka:** Conceptualization, Methodology, Writing – review & editing, Supervision, Project administration.

Declaration of competing interest

The authors declare that they have no known competing financial interests or personal relationships that could have appeared to influence the work reported in this paper.

Acknowledgements

Financial assistance provided by Grant agreement ID: 823969 funded by the European Commission within H2020 MSCA-RISE research fund is acknowledged here. Scientific work co-financed from the budged for science in the years 2019–2020 by Grant agreement 5020/H2020/2019/2 funded by Ministry of Science and Higher Education of Poland under the PMW programme.

References

[1] Gnacinski P. Prediction of windings temperature rise in induction motors supplied with distorted voltage. Energy Convers Manage 2008;49(4):707–17. http://dx.doi.org/10.1016/j.enconman.2007.07.023.

[2] British Standards Institute. IEC 60076-7:2018: Power transformers. Loading guide for mineral-oil-immersed power Transformers. 2018.

[3] Abu-Elanien AE, Salama M. A Monte Carlo approach for calculating the thermal lifetime of transformer insulation. Int J Electr Power Energy Syst 2012;43(1):481–7. http://dx.doi.org/10.1016/j.ijepes.2012.06.054.

[4] Rafiq M, Lv YZ, Zhou Y, Ma KB, Wang W, Li CR, Wang Q. Use of vegetable oils as transformer oils-A review. Renew Sustain Energy Rev 2015;52:308–24. http://dx.doi.org/10.1016/j.rser.2015.07.032.

[5] Dombek G, Goscinski P, Nadolny Z. Comparison of mineral oil and esters as cooling liquids in high voltage transformer in aspect of environment protection. E3S Web Conf 2017;14. http://dx.doi.org/10.1051/e3sconf/20171401053.

[6] Salama MMM, Mansour DEA, Daghrah M, Abdelkasoud SM, Abbas AA. Thermal performance of transformers filled with environmentally friendly oils under various loading conditions. Int J Electr Power Energy Syst 2020;118:105743. http://dx.doi.org/10.1016/j.ijepes.2019.105743.

[7] Cilliyuz Y, Bicen Y, Aras F, Aydugan G. Measurements and performance evaluations of natural ester and mineral oil-immersed identical transformers. Int J Electr Power Energy Syst 2021;125:106517. http://dx.doi.org/10.1016/j.ijepes.2020.106517.

[8] Ortiz A, Delgado F, Ortiz F, Fernández I, Santisteban A. The aging impact on the cooling capacity of a natural ester used in power transformers. Appl Therm Eng 2018;144(April):797–803. http://dx.doi.org/10.1016/j.applthermaleng.2018.08.049.

[9] Villarroel R, García de Burgos B, García DF. Moisture dynamics in natural-ester filled transformers. Int J Electr Power Energy Syst 2021;124:106172. http://dx.doi.org/10.1016/j.ijepes.2020.106172.

[10] Raeisian L, Niazmand H, Ebrahimnia-Bajestan E, Werle P. Feasibility study of waste vegetable oil as an alternative cooling medium in transformers. Appl Therm Eng 2019;151(September 2018):308–17. http://dx.doi.org/10.1016/j.applthermaleng.2019.02.010.

[11] Zhou LJ, Wu GN, Yu JF, Zhang XH. Thermal overshoot analysis for hot-spot temperature rise of transformer. IEEE Trans Dielectr Electr Insul 2007;14(5):1316–22. http://dx.doi.org/10.1109/TDEI.2007.4339495.

[12] Radakovic Z, Jevtic M, Das B. Dynamic thermal model of kiosk oil immersed transformers based on the thermal buoyancy driven air flow. Int J Electr Power Energy Syst 2017;92:14–24. http://dx.doi.org/10.1016/j.ijepes.2017.04.003.

[13] Taghikhani MA, Gholami A. Prediction of hottest spot temperature in power transformer windings with non-directed and directed oil-forced cooling. Int J Electr Power Energy Syst 2009;31(7–8):356–64. http://dx.doi.org/10.1016/j.ijepes.2009.03.009.

[14] Rommel DP, Di Maio D, Tinga T. Transformer hot spot temperature prediction based on basic operator information. Int J Electr Power Energy Syst 2021;124:106340. http://dx.doi.org/10.1016/j.ijepes.2020.106340.

[15] Shiravand V, Faiz J, Samimi MH, Djamali M. Improving the transformer thermal modeling by considering additional thermal points. Int J Electr Power Energy Syst 2021;128:106748. http://dx.doi.org/10.1016/j.ijepes.2020.106748.

[16] Smolka J, Ingham DB, Elliott L, Nowak AJ. Enhanced numerical model of performance of an encapsulated three-phase transformer in laboratory environment. Appl Therm Eng 2007;27(1):156–66. http://dx.doi.org/10.1016/j.applthermaleng.2006.05.008.

[17] Eslamian M, Vahidi B, Hosseinian SH. Analytical calculation of detailed model parameters of cast resin dry-type transformers. Energy Convers Manage 2011;52(7):2565–74. http://dx.doi.org/10.1016/j.enconman.2011.01.011.

[18] Rahimpour E, Barati M, Schäfer M. An investigation of parameters affecting the temperature rise in windings with zigzag cooling flow path. Appl Therm Eng 2007;27(11–12):1923–30. http://dx.doi.org/10.1016/j.applthermaleng.2006.12.019.

[19] Santisteban A, Fernández FO, Fernández I, Delgado F, Ortiz A, Renedo CJ. Thermal analysis of natural esters in a low-voltage disc-type winding of a power transformer. In: 2017 IEEE 19th international conference on dielectric liquids (ICDL). 2017, p. 1–4. http://dx.doi.org/10.1109/ICDL.2017.8124698.

[20] Torriano F, Chaaban M, Picher P. Numerical study of parameters affecting the temperature distribution in a disc-type transformer winding. Appl Therm Eng 2010;30(14–15):2034–44. http://dx.doi.org/10.1016/j.applthermaleng.2010.05.004.

[21] Skillen A, Revell A, Iacovides H, Wu W. Numerical prediction of local hot-spot phenomena in transformer windings. Appl Therm Eng 2012;36(1):96–105. http://dx.doi.org/10.1016/j.applthermaleng.2011.11.054.

[22] Gastelurrutia J, Ramos JC, Larraona GS, Rivas A, Izagirre J, Del Río L. Numerical modelling of natural convection of oil inside distribution transformers. Appl Therm Eng 2011;31(4):493–505. http://dx.doi.org/10.1016/j.applthermaleng.2010.10.004.

[23] Torriano F, Picher P, Chaaban M. Numerical investigation of 3D flow and thermal effects in a disc-type transformer winding. Appl Therm Eng 2012;40:121–31. http://dx.doi.org/10.1016/j.applthermaleng.2012.02.011.

[24] Eslamian M, Vahidi B, Eslamian A. Thermal analysis of cast-resin dry-type transformers. Energy Convers Manage 2011;52(7):2479–88. http://dx.doi.org/10.1016/j.enconman.2011.02.006.

[25] Ríos Rodriguez G, Garelli L, Storti M, Granata D, Amadei M, Rossetti M. Numerical and experimental thermo-fluid dynamic analysis of a power transformer working in ONAN mode. Appl Therm Eng 2017;112:1271–80. http://dx.doi.org/10.1016/j.applthermaleng.2016.08.171.

[26] Garelli L, Ríos Rodriguez G, Storti M, Granata D, Amadei M, Rossetti M. Reduced model for the thermo-fluid dynamic analysis of a power transformer radiator working in ONAF mode. Appl Therm Eng 2017;124:855–64. http://dx.doi.org/10.1016/j.applthermaleng.2017.06.098.

[27] Kim YJ, Jeong M, Park YG, Ha MY. A numerical study of the effect of a hybrid cooling system on the cooling performance of a large power transformer. Appl Therm Eng 2018;136:275–86. http://dx.doi.org/10.1016/j.applthermaleng.2018.03.019.

[28] Raeisian L, Niazmand H, Ebrahimnia-Bajestan E, Werle P. Thermal management of a distribution transformer: An optimization study of the cooling system using CFD and response surface methodology. Int J Electr Power Energy Syst 2019;104:443–55. http://dx.doi.org/10.1016/j.ijepes.2018.07.043.

[29] Smolka J, Nowak AJ. Shape optimization of coils and cooling ducts in dry-type transformers using computational fluid dynamics and genetic algorithm. IEEE Trans Magn 2011;47(6):1726–31. http://dx.doi.org/10.1109/TMAG.2011.2109731.

[30] Smolka J. CFD-based 3-D optimization of the mutual coil configuration for the effective cooling of an electrical transformer. Appl Therm Eng 2013;50(1):124–33. http://dx.doi.org/10.1016/j.applthermaleng.2012.06.012.

[31] Smolka J, Nowak AJ. Experimental validation of the coupled fluid flow, heat transfer and electromagnetic numerical model of the medium-power dry-type electrical transformer. Int J Therm Sci 2008;47(10):1393–410. http://dx.doi.org/10.1016/j.ijthermalsci.2007.11.004.

[32] El Wakil N, Chereches N-C, Padet J. Numerical study of heat transfer and fluid flow in a power transformer. Int J Therm Sci 2006;45(6):615–26. http://dx.doi.org/10.1016/j.ijthermalsci.2005.09.002.

[33] Bíró O. Edge element formulation of eddy current problems. Comput Methods Appl Mech Engrg 1999;169:391–405. http://dx.doi.org/10.1016/S0045-7825(98)00165-0.

[34] Ozturk N, Celik E. Application of genetic algorithms to core loss coefficient extraction. Prog Electromagn Res M 2011;19:133–46. http://dx.doi.org/10.2528/pierm11051310.

[35] Versteeg HK, Malalasekara W. An introduction to computational fluid dynamics: The finite volume method. Harlow: Pearson Education; 2007.

[36] Hey J, Malloy AC, Martinez-Botas R, Lamperth M. Conjugate heat transfer analysis of an energy conversion device with an updated numerical model obtained through inverse identification. Energy Convers Manage 2015;94:198–209. http://dx.doi.org/10.1016/j.enconman.2015.01.065.

[37] Xue S, Feng J, Guo S, Peng J, Chu WQ, Zhu ZQ. A new iron loss model for temperature dependencies of hysteresis and eddy current losses in electrical machines. IEEE Trans Magn 2018;54. http://dx.doi.org/10.1109/tmag.2017.2755593.

[38] Santisteban A, Piquero A, Ortiz F, Delgado F, Ortiz A. Thermal modelling of a power transformer disc type winding immersed in mineral and ester-based oils using network models and CFD. IEEE Access 2019;7:174651–61. http://dx.doi.org/10.1109/ACCESS.2019.2957171.

[39] Climate-data, Climate data for cities worldwide, https://en.climate-data.org.

[40] Churchill SW, Chu HHS. Correlating equations for laminar and turbulent free convection from a vertical plate. Int J Heat Mass Transfer 1975;18(11):1323–9. http://dx.doi.org/10.1016/0017-9310(75)90243-4.

[41] Lloyd JR, Morgan WR. Natural convection adjacent to horizontal surface of various platforms. ASME J Heat Transfer 1974;96(4):443–7. http://dx.doi.org/10.1115/1.3450224.

[42] Cengel YA. Heat transfer: A practical approach. 3rd ed.. New York: McGraw-Hill; 2002.